RANDOM ENCODING TECHNIQUES USING DARK–BRIGHT SOLITON CONVERSION WITH MZI INCORPORATING MICRORING RESONATORS

CHAT TEEKA

A THESIS SUBMITTED IN FULFILLMENT

OF THE REQUIREMENT FOR THE DEGREE OF

DOCTOR OF PHILOSOPHY IN APPLIED PHYSICS

FACULTY OF SCIENCE

KING MONGKUT'S INSTITUTE OF TECHNOLOGY LADKRABANG

2011

KMITL-2011-SC-D-030-028

หัวข้อวิทยานิพนธ์	**เทคนิคการเข้ารหัสแบบสุ่มโดยใช้การแปลงกลับดาร์ค–ไบร์ทโซลิตอนในเอ็มแซทไอร่วมกับโพรงสั่นพ้องแบบวงแหวนระดับไมโครเมตร**
นักศึกษา	**นายชาติ ทีฆะ**
รหัสประจำตัว	52650106
ปริญญา	**ปรัชญาดุษฎีบัณฑิต**
สาขาวิชา	**ฟิสิกส์ประยุกต์**
พ.ศ.	2554
อาจารย์ที่ปรึกษา	**รองศาสตราจารย์ ดร. ปรีชา ยุพาพิน**

บทคัดย่อ

งานวิจัยนี้เป็นการนำเสนอเทคนิคการเข้ารหัสแบบสุ่มโดยใช้การแปลงกลับดาร์ค–ไบร์ทโซลิตอนใน MZI ร่วมกับโพรงสั่นพ้องแบบวงแหวนระดับไมโครเมตร สัญญาณแสงแบบไม่เป็นเชิงเส้นที่เกิดขึ้นใน MZI สามารถสร้างเทคนิคการปิด–เปิดเชิงแสงได้ ขั้นตอนแรกเป็นการวิเคราะห์หลักการเข้ารหัสแบบเฟสโดยการควบคุมการเปลี่ยนเฟสในลักษณะสวิตช์ปิด–เปิดในระบบ MZI รวมเข้ากับโพรงสั่นพ้องชนิดไม่เป็นเชิงเส้นแบบวงแหวน 3 วงแหวน ขั้นตอนที่สองเป็นการศึกษาพฤติกรรมการเดินทางของสัญญาณแสงชนิดดาร์ค–ไบร์ทโซลิตอนที่ชนกันภายในระบบตัวกรองเชิงแสงชนิดแอดครอปที่สร้างขึ้นซึ่งเราเรียกว่าโพรงสั่นพ้องแบบวงแหวนชนิดแพนด้า โดยการควบคุมการแปลงกลับดาร์ค–ไบร์ทโซลิตอนภายในระบบพบว่าสามารถสร้างสัญญาณเชิงแสงในรูปแบบไบนารีโค้ดแบบสุ่มในระบบโพรงสั่นพ้องแบบวงแหวนชนิดแพนด้าซึ่งสามารถนำไปประยุกต์ใช้กับระบบความปลอดภัยในการสื่อสารเชิงแสง ในขณะที่การถอดรหัสสามารถทำได้โดยใช้หลักการแปลงกลับดาร์ค–ไบร์ทโซลิตอนในระบบตัวกรองเชิงแสงชนิดแอดครอป ขั้นตอนสุดท้ายเป็นการประยุกต์ใช้หลักการการแปลงกลับดาร์ค–ไบร์ทโซลิตอนในการสร้างคีบจับเชิงแสง สัญญาณคีบจับเชิงแสงที่สร้างขึ้นนี้สามารถปรับขยายแอมพลิจูดและความกว้างของบ่อคีบจับโดยการควบคุมดาร์คโซลิตอนที่ครอปพอร์ตของตัวกรองเชิงแสงชนิดแอดครอป สัญญาณคีบจับเชิงแสงที่สร้างขึ้นนี้สามารถนำไปคีบจับสัญญาณหรืออะตอม

คำสำคัญ : เทคนิคการเข้ารหัสแบบสุ่ม, โซลิตอน, โพรงสั่นพ้องแบบวงแหวนระดับไมโครเมตร, โพรงสั่นพ้องแบบวงแหวนชนิดแพนด้า, คีบจับเชิงแสง

Thesis Title	Random Encoding Techniques using Dark–Bright Soliton Conversion with MZI Incorporating Microring Resonators
Student	Chat Teeka
Student ID	52650106
Degree	Doctor of Philosophy
Program	Applied Physics
Year	2011
Thesis Advisor	Assoc. Prof. Dr. Preecha Yupapin

ABSTRACT

This thesis presents the novel random encoding techniques using dark–bright soliton conversion with MZI incorporating microring resonators. The nonlinear light pulse is propagation within a Mach–Zehnder Interferometer (MZI) which can be used to extend the existed on–off keying (OOK) techniques. First, the principles of a phase modulation scheme using MZI incorporating the triple nonlinear ring resonators is analyzed, which can be fabricated and used in practical communications. I focus on the recent modulation schemes, where the all-optical on–off keying and the phase shift control for phase shaped binary transmission (PSBT) are discussed in details. The novelty of this work is that the nonlinear ring resonators are used incorporating a MZI, where the extended switching generation can be achieved and seen.

Secondary, the dynamic behavior of dark–bright soliton collision within the modified add/drop filter, which it is known as PANDA ring resonator. By using the dark–bright soliton conversion control, the obtained outputs of the dynamic states can be used to form the random binary codes, which can be available for communication security application. Results obtained have shown that the random binary codes can be formed by using the polarized light components, whereas the retrieved (decoded) codes can be obtained by using the dark–bright soliton conversion signals.

Finally, I propose a novel system of the tunable dynamic optical tweezers using a generated dark soliton in the fiber optic loop. A dark soliton known as an optical tweezers is amplified and tuned within the ring resonator system. The required tunable tweezers with different width and power can be controlled. The control dark soliton is input into the system via the add port of the add/drop filter, where the dynamic behavior of the dark–bright soliton conversion is seen. The required stable signal is obtained via a drop and throughput ports of the add/drop filter with some suitable parameters. In application, the dynamic optical tweezers can be configured by the dark–bright soliton conversion system. Therefore, the use of trapped light/atom can be covered by using the proposed system.

Keywords: random encoding technique, dark–bright soliton conversion, MZI, microring resonator, PANDA ring resonators and optical tweezers.

ACKNOWLEDGEMENTS

While I have worked on this thesis for over three years, several people have contributed to this effort directly and indirectly. I would like to express my thankfulness to all of them.

No student thesis is achievable without the guidance and assistance of the thesis advisor. I was fortunate to have Assoc. Prof. Dr. Preecha P. Yupapin as my thesis advisor. His patient guidance, encouragement and enthusiasm throughout the development of my thesis were highly prized.

My profound gratitude must go to my parents, my wife, and my baby for infinite encouraging and understanding me. They have always been there for me with this thesis. With their love, my thesis has been possible. Special thanks are due to my best friends (ARCP) for their support. Some of them shared my insanity of doing a doctoral degree.

I would like to acknowledge Suan Dusit Rajabhat University, Bangkok, Thailand for granting the Thailand Ph.D. Program at Faculty of Science, King Mongkut's Institute of Technology Ladkrabang, Bangkok, Thailand.

TABLE OF CONTENTS

Pages

LIST OF TABLES

Pages

LIST OF FIGURES

Figures **Pages**

CHAPTER 1

INTRODUCTION

1.1 On–Off Keying Generation

Today, most of the optical communication links use the well known modulation format called OOK (On–Off Keying) [1 – 9], which is due to the increasing in bit rates, power and number of DWDM (Dense Wavelength Division Multiplexing) channels, where the OOK format can reach the communication requirement. However, the various modulation schemes have already been used in the electrical domain during last decade, but they have not been applied in optical schemes. Recently the use of new modulation formats in optical communications has been considered and compared for increasing the tolerance of the optical link to impairments such as chromatic dispersion, PMD (Polarization mode dispersion) or nonlinearity (Kerr Effect) [10]. Among the various modulation formats, we present here the differential phase shift keying (DPSK) and the phase shaped binary transmission (PSBT) schemes, whereas DPSK presents a better robustness to optical nonlinearities than the classical OOK, particularly for the cross phase modulation (XPM) in DWDM systems [3, 9, 11]. Moreover, it has also been shown that DPSK format has better performances due to PMD degradations than the classical OOK [9, 11]. The disadvantage of the DPSK is that a direct detection (DD) at the end of the optical link is not possible, since DPSK is a phase modulation. Thus, an interferometric demodulation stage must be inserted in front of the photo-detector. This stage is an "Add and Delay" structure, which is composed by a MZI [9, 11 – 15].

In this section, my first describe the principles of light propagation in the proposed system, where the nonlinear behavior of light within the nonlinear ring resonators (NRRs) can be used to analyze for PSBT modulation. After that, the MZI structure is detailed. However, the nonlinear ring resonator has been used [16 – 19] for phase shifted generate by couple to one arm of a MZI

[16 – 17]. In this structure, one arm presents an optical delay line equal to the bit duration. This MZI converts an optical DPSK to an intensity–modulated (IM) signal, which is followed by a DD. The PSBT format is encoded from a DPSK: first a DPSK signal is generated and after that a MZI structure converts the DPSK to be an intensity–modulated signal: the PSBT. MZI characteristics for the two applications are slightly different, as will see in the next sections. The novelty of this work is that the nonlinear light pulses generated by using the triple nonlinear ring resonators in one arm of a Mach–Zehnder interferometer can be used to enhance (amplify) the light pulse output signals, where the nonlinear outputs are generated by using the nonlinear coefficient refractive index $n_2 = 2.2\times10^{-13}\ m^2/W$.

1.2 Novel Tunable Dynamic Tweezers

Optical tweezers are a powerful tool for use in the three–dimensional rotation of and translation (location manipulation) of nano–structures such as micro- and nano–particles as well as living microorganisms [20]. The benefit offered by optical tweezers is the ability to interact with nano–scaled objects in a non–invasive manner, i.e. there is no physical contact with the sample, thus preserving many important characteristics of the sample, such as the manipulation of a cell with no harm to the cell. Optical tweezers are now widely used and they are particularly powerful in the field of microbiology [21 – 24] to study cell–cell interactions, manipulate organelles without breaking the cell membrane and to measure adhesion forces between cells. To make the familiarity for such a new combination area, firstly, the theoretical description of optical soliton is reviewed, where more details can also be found in many references, especially, one of them which are well analyzed by Agrawal [25]. Secondly, a new concept of developing an optical tweezers source using a dark soliton pulse is demonstrated. The developed tweezers has many potential applications in electron, ion, atom and molecule probing and manipulation as well as DNA probing and transportation [26, 27]. Furthermore, the soliton pulse generator is a simple and compact design, making it more commercially viable. In principle, the change in potential value, i.e. gradient of potential of the dark soliton pulse can produce force that can be used to

confine/trap atoms/molecule. Furthermore, the change in potential well is still stable in some conditions, which mean that the dynamic optical tweezers is plausible. Finally, we present the very interesting work of the use of a dark soliton pulse beam that has potential applications in the probing and transport of atoms or molecules as an optical tweezers, which is important to ensure that the transported atom/molecule is not lost in the link media. The theoretical background of the trapped atom/molecule is also analyzed and described in details. The system design of the tweezers amplification, tunable and storage is also analyzed for the use of atom/molecule probing and assembly.

In this section, the dark soliton pulse was experimentally generated using a pumped fiber optic loop. The obtained dark soliton can be amplified and tuned by using the nonlinear ring resonator system analytically. The tunable tweezers (dark soliton) is controlled by using the dark–bright soliton conversion control. The dynamic behaviors of soliton conversion, i.e. tunable optical tweezers within an add/drop filter is analyzed. The multiplexed signals with different wavelengths into the system is also available via the add port, which means the use of atom/molecule transportation in the network is possible.

1.3 Low Power Ultrafast Switching Generation

All-optical switches have been extensively investigated for the implementation of the ultrafast optical networks, especially, when the high capacity data transmission is required, in which the use ultrafast switching based on photonic crystal nanocavity [28, 29], spin–polarized surface–normal optical switches [30] and digital optical circuits and their use in packet switching [31] have been reported. However, the switching operation improvements are still required, here, the improvement of orthogonal ASK/DPSK optical label switching performance by DC–balanced line encoding [32] and low threshold and tunable all–optical switch using two-photon absorption in array of nonlinear ring resonators coupled to MZI [17] are included. More research works in various schemes are also included, for instance, the use of all–optical ultrafast switching can be controlled by using a high–nonlinear micro ring coupled MZI through a pumped nonlinear

coupler [18], an EDF–ring coupled M–Z interferometer [33], asymmetric Fano resonance and bistability for high extinction ratio, large modulation depth, and low power switching [34], THz electro–absorption effect enabling femtosecond all–optical switching in semiconductor quantum dots [35], nanosecond switching and wavelength tuning of external–cavity laser diode using a reflective electro–absorption modulator [36], detailed design and characterization of all–optical switches based on InAs/GaAs quantum dots in a vertical cavity [37], threshold voltage and mobility extraction by ultrafast switching measurement on NBTI [38]. Till date, the ultrafast switching improvement, especially, ultrafast packet switching is still required. Recently, the ultrafast packet switching generation using a nonlinear microring resonator for secure packet switching application has been proposed, where more recently, the use of OOK ultrafast switching generation based on MZI incorporating a pumped nonlinear ring resonators system [39] has also been reported, in which the reports of switching speeds for such devices are on the order of *ps*.

In this section, I propose a scheme for generating ultrafast switching with low power input based on nonlinear microring resonators (NMRs) coupled into a MZI arm. In order to increase the bit–rate of on–chip optical links by using FDTD method [40], in which the nonlinear behavior of light within the (NMRs) can be used to analyze for low power ultrafast switching modulation. The NMRs are coupled into a MZI arm structure and the details given. Moreover, the NMRs are used for a phase shifted devices by coupling into one arm of a MZI [39]. In this structure, one arm presents an optical delay line equal to the bit duration time. The MZI characteristics for the two applications are slightly different, which will be seen in the next sections. The novelty of this work is that the nonlinear light pulses generated by using the multi NMRs in one arm of a Mach–Zehnder interferometer can be used to enhance (amplify) the packet switching signals, where the increasing in switching sped and delay switching time can be obtained by using the coupled nonlinear ring resonators, where in this work the nonlinear coefficient refractive index of nonlinear ring resonator (GaInAsP/InP) is $n_2 = 2.2\times10^{-13}\ m^2/W$.

1.4 Objective

The objectives of the research are following

1.4.1 To study and understand the OOK generation based on MZI incorporating a pumped nonlinear ring resonators system.

1.4.2 To study and understand the random binary code generation using dark–bright soliton conversion control within a PANDA ring resonator.

1.4.3 To study a tunable dynamic tweezers using dark–bright solitons collision control in an optical add/drop filter.

1.4.4 To study the low power ultrafast switching generation based on NMRs coupled into a MZI arm.

1.5 Scope of the Research

This thesis presents the novel random encoding techniques using dark–bright soliton conversion with MZI incorporating microring resonators. The nonlinear light pulse is propagation within a Mach–Zehnder Interferometer (MZI) which can be used to extend the existed on–off keying (OOK) techniques. First, the principles of a phase modulation scheme using MZI incorporating the triple nonlinear ring resonators is analyzed, which can be fabricated and used in practical communications. I focus on the recent modulation schemes, where the all–optical on–off keying and the phase shift control for phase shaped binary transmission (PSBT) are discussed in details. The novelty of this work is that the nonlinear ring resonators are used incorporating a MZI, where the extended switching generation can be achieved and seen.

Secondary, the dynamic behavior of dark–bright soliton collision within the modified add/drop filter, which it is known as PANDA ring resonator. By using the dark–bright soliton conversion control, the obtained outputs of the dynamic states can be used to form the random

binary codes, which can be available for communication security application. Results obtained have shown that the random binary codes can be formed by using the polarized light components, whereas the retrieved (decoded) codes can be obtained by using the dark–bright soliton conversion signals.

Finally, I propose a novel system of the tunable dynamic optical tweezers using a generated dark soliton in the fiber optic loop. A dark soliton known as an optical tweezers is amplified and tuned within the ring resonator system. The required tunable tweezers with different width and power can be controlled. The control dark soliton is input into the system via the add port of the add/drop filter, where the dynamic behavior of the dark–bright soliton conversion is seen. The required stable signal is obtained via a drop and throughput ports of the add/drop filter with some suitable parameters. In application, the dynamic optical tweezers can be configured by the dark–bright soliton conversion system. Therefore, the use of trapped light/atom can be covered by using the proposed system.

CHAPTER 2

THEORETICAL BACKGROUND

2.1 Microring Coupler to Mach–Zehnder Interferometer

Figure 2.1 shows the proposal for on–off keying model using nonlinear index of refraction in three nonlinear ringresonator coupled to one arm of Mach–Zehnder interferometer. In this figure there are similar NRRs with the field–dependent absorption and index of refraction coefficients.

When the input field, E_{in}, passes through 3dB coupler with coupling coefficient ratio, K_1, 50:50, then light is split into two ways, which can be expressed as

$$E_{11} = \sqrt{1-\gamma_1}\sqrt{1-\kappa_1}E_{in}, \tag{2.1}$$

$$E_{21} = j\sqrt{1-\gamma_1}\sqrt{\kappa_1}E_{in}, \tag{2.2}$$

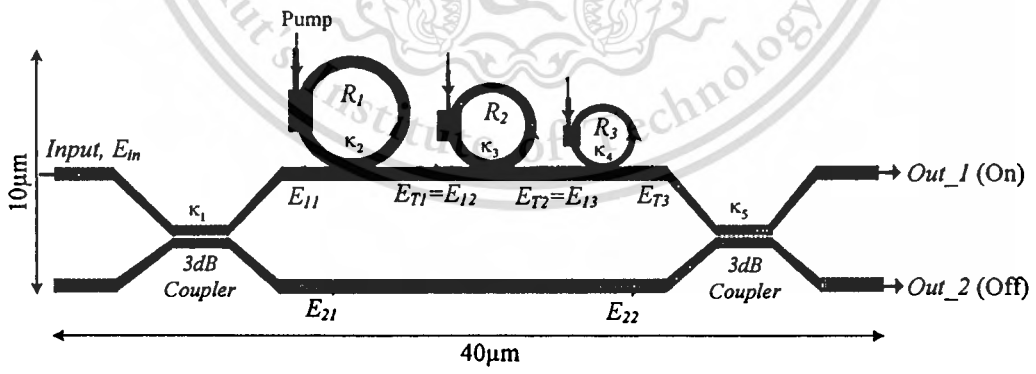

Figure 2.1 Schematic diagram of OOK system, system size is $10 \times 40\mu m^2$.

According to the linear coupling theory, the following relations can connect input–output fields for each nonlinear ring resonators (NRRs) as shown in figure 2.2, which can be expressed by [17]

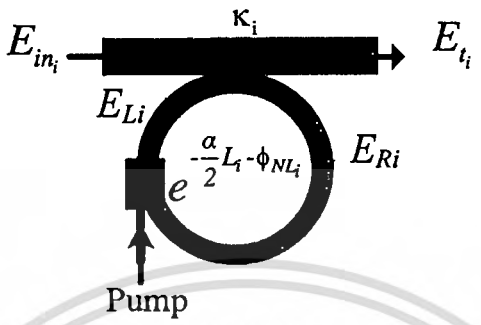

Figure 2.2 Schematic diagram of single NRR (i = 2, 3, 4).

$$E_{Ri} = \sqrt{1-\gamma_i}\sqrt{1-\kappa_i}E_{Li} + j\sqrt{1-\gamma_i}\sqrt{\kappa_i}E_{in_i}, \tag{2.3}$$

$$E_{t_i} = \sqrt{1-\gamma_i}\sqrt{1-\kappa_i}E_{in_i} + j\sqrt{1-\gamma_i}\sqrt{\kappa_i}E_{Li}, \tag{2.4}$$

where γ_i and κ_i are the coupler loss and coupling coefficient in each NRR, respectively. Since the NRR length and the nonlinear index of refraction are small, therefore, the nonlinear Schrodinger equation (NLS) can be used to solve light propagation through the NRRs, the solution is given by [17]

$$E_{Li} = E_{Ri}\exp\left(-\frac{\alpha}{2}L_i - \gamma_{NL_i}\left|E_{Ri}\right|^2 L_i\right). \tag{2.5}$$

where α, $L_i = 2\pi R_i$ and γ_{NL_i} are the NRR loss, NRR length (R_i is ring radius) and the nonlinear coefficient including the nonlinear index of refraction and two–photon absorption phenomenon, respectively. By using the basic concepts in nonlinear optics, the following relation can be used for the above mentioned, the nonlinear coefficient is given by

$$\gamma_{NL_i} = \frac{\beta}{2} - j\frac{\omega_0}{c}n_2 \tag{2.6}$$

where β, ω_0, C and n_2 are the two–photon absorption coefficient, incident light frequency, speed of light in free space and the nonlinear index of refraction coefficient, respectively. The following relation describes the nonlinear phenomenon in the NRRs as

$$\begin{aligned}\tilde{\alpha} &= \alpha + \beta|E|^2, \\ \tilde{n} &= n + n_2|E|^2,\end{aligned} \tag{2.7}$$

where both of the absorption coefficient and index of refraction includes linear and nonlinear parts and the following relations can be used for obtaining these variables in terms of the optical third order susceptibility as

$$\begin{aligned}n_2 &= \frac{3}{8n}\mathrm{Re}\left[\chi^{(3)}\right], \\ \beta &= \frac{3\omega_0}{4nC}\mathrm{Im}\left[\chi^{(3)}\right].\end{aligned} \tag{2.8}$$

Using Eqs. (2.3) – (2.5) and some mathematical manipulations, the following transmission functions can be obtained for each NRRs as

$$T = \frac{E_{t_i}}{E_{in_i}} = \sqrt{1-\gamma_i}\sqrt{1-\kappa_i} - \frac{\kappa_i(1-\gamma_i)\exp\left(-\frac{\alpha}{2}L_i - \phi_{NL_i}\right)}{1-\sqrt{1-\gamma_i}\sqrt{1-\kappa_i}\exp\left(-\frac{\alpha}{2}L_i - \phi_{NL_i}\right)}. \tag{2.9}$$

where $\phi_{NL_i} = \gamma_{NL_i}L_i|E_{Ri}|^2$ is defined as a nonlinear phase shift.

For the obtained result in Eq. (2.9), the phase difference (effective phase from single NRR) can be found as follows:

$$\phi_{eff} = \phi_i = \tan^{-1}\left[\frac{-\kappa_i(1-\gamma_i)e^{-1/2\left(\alpha+\beta|E_{Ri}|^2\right)L_i}\times\sin\left((\omega_0/C)n_2L_i|E_{Ri}|^2\right)}{A+B+D}\right], \tag{2.10}$$

where $A=(2-\kappa_i)(1-\gamma_i)e^{-1/2\left(\alpha+\beta|E_{Ri}|^2\right)L_1}\cos\left((\omega_0/C)n_2L_1|E_{Ri}|^2\right)$, $B=\sqrt{(1-\kappa_i)(1-\gamma_i)}$ and $D=(1-\gamma_i)\sqrt{(1-\kappa_i)(1-\gamma_i)}e^{-\left(\alpha+\beta|E_{Ri}|^2\right)L_1}$.

The obtained result can be simplified to the following formula, which is assumed by $\gamma_i=\alpha=\beta=0$.

$$\phi_{eff}=\phi_i=\tan^{-1}\left[\frac{-\kappa_i\sin\left(\frac{\omega_0}{C}n_2L_1|E_{Ri}|^2\right)}{2\sqrt{1-\kappa_i}-(2-\kappa_i)\cos\left(\frac{\omega_0}{C}n_2L_1|E_{Ri}|^2\right)}\right]. \tag{2.11}$$

In real system $\gamma_i,\alpha,$ and β are not be zero as shown in section 3, $\alpha = 0.5dBmm^{-1}$, $\gamma=0.1$ and $\beta= 2\times10^{-11}$, respectively.

And, the output power at light propagation through the first NRR is given by

$$\frac{P_{t1}}{P_{in}}=\left|\frac{E_{t1}}{E_{in}}\right|^2. \tag{2.12}$$

The electric field of light propagation through the second NRR is given by

$$\frac{E_{t2}}{E_{in}}=\frac{\sqrt{1-\gamma_1}\sqrt{1-\gamma_2}\sqrt{1-\gamma_3}\sqrt{1-\kappa_1}\left(\begin{array}{l}\sqrt{1-\kappa_2}\sqrt{1-\kappa_3}-\sqrt{1-\gamma_2}\sqrt{1-\kappa_3}e^{-\frac{\alpha}{2}L_1-\phi_{NL,1}}\\-\sqrt{1-\gamma_3}\sqrt{1-\kappa_2}\,e^{-\frac{\alpha}{2}L_2-\phi_{NL,2}}\\+\sqrt{1-\gamma_2}\sqrt{1-\gamma_3}\,e^{-\frac{\alpha}{2}(L_1+L_2)-(\phi_{NL,1}+\phi_{NL,2})}\end{array}\right)}{\left(\begin{array}{l}1+\sqrt{1-\gamma_2}\sqrt{1-\kappa_2}\,e^{-\frac{\alpha}{2}L_1-\phi_{NL,1}}-\sqrt{1-\gamma_3}\sqrt{1-\kappa_3}\,e^{-\frac{\alpha}{2}L_2-\phi_{NL,2}}\\+\sqrt{1-\gamma_2}\sqrt{1-\gamma_3}\sqrt{1-\kappa_2}\sqrt{1-\kappa_3}\,e^{-\frac{\alpha}{2}(L_1+L_2)-(\phi_{NL,1}+\phi_{NL,2})}\end{array}\right)}, \tag{2.13}$$

where $\sqrt{1-\gamma_1}$, $\sqrt{1-\gamma_2}$, $\sqrt{1-\gamma_3}$, $\sqrt{1-\gamma_4}$ and $\sqrt{1-\gamma_5}$ are coupler losses in each coupler and $\sqrt{1-\kappa_1}$, $\sqrt{1-\kappa_2}$, $\sqrt{1-\kappa_3}$, $\sqrt{1-\kappa_4}$ and $\sqrt{1-\kappa_5}$ are coupler separates in each coupler, respectively.

The output power of light propagation through the second NRR is given by

$$\frac{P_{t2}}{P_{in}}=\left|\frac{E_{t2}}{E_{in}}\right|^2. \tag{2.14}$$

The electric field of light propagation through third NRR the relation input–output field is

$$\frac{E_{t3}}{E_{in}}=\frac{A\begin{pmatrix}\sqrt{1-\kappa_2}\sqrt{1-\kappa_3}\sqrt{1-\kappa_4}\\ -\sqrt{1-\kappa_3}\sqrt{1-\kappa_4}\,e^{-\frac{\alpha}{2}L_1-\phi_{NL,1}}\\ -\sqrt{1-\kappa_2}\sqrt{1-\kappa_4}\,e^{-\frac{\alpha}{2}L_2-\phi_{NL,2}}\\ +\sqrt{1-\kappa_4}\,e^{-\frac{\alpha}{2}(L_1+L_2)-(\phi_{NL,1}+\phi_{NL,2})}\\ -\sqrt{1-\kappa_2}\sqrt{1-\kappa_3}\,e^{-\frac{\alpha}{2}L_3-\phi_{NL,3}}\\ +\sqrt{1-\kappa_3}\,e^{-\frac{\alpha}{2}(L_1+L_3)-(\phi_{NL,1}+\phi_{NL,3})}\\ +\sqrt{1-\kappa_2}\,e^{-\frac{\alpha}{2}(L_2+L_3)-(\phi_{NL,2}+\phi_{NL,3})}\\ +\sqrt{1-\kappa_3}\sqrt{1-\kappa_4}\,e^{-\frac{\alpha}{2}(L_1+L_2+L_3)-(\phi_{NL,1}+\phi_{NL,2}+\phi_{NL,3})}\end{pmatrix}}{\begin{pmatrix}1+\sqrt{1-\gamma_2}\sqrt{1-\kappa_2}\,e^{-\frac{\alpha}{2}L_1-\phi_{NL,1}}\\ -\sqrt{1-\gamma_3}\sqrt{1-\kappa_3}\,e^{-\frac{\alpha}{2}L_2-\phi_{NL,2}}-\sqrt{1-\gamma_4}\sqrt{1-\kappa_4}\,e^{-\frac{\alpha}{2}L_3-\phi_{NL,3}}\\ +\sqrt{1-\gamma_2}\sqrt{1-\gamma_3}\sqrt{1-\kappa_2}\sqrt{1-\kappa_3}\,e^{-\frac{\alpha}{2}(L_1+L_2)-(\phi_{NL,1}+\phi_{NL,2})}\\ +\sqrt{1-\gamma_3}\sqrt{1-\gamma_4}\sqrt{1-\kappa_3}\sqrt{1-\kappa_4}\,e^{-\frac{\alpha}{2}(L_2+L_3)-(\phi_{NL,2}+\phi_{NL,3})}\\ -\sqrt{1-\gamma_2}\sqrt{1-\gamma_3}\sqrt{1-\gamma_4}\sqrt{1-\kappa_2}\sqrt{1-\kappa_3}\sqrt{1-\kappa_4}\\ \times e^{-\frac{\alpha}{2}(L_1+L_2+L_3)-(\phi_{NL,1}+\phi_{NL,2}+\phi_{NL,3})}\end{pmatrix}}, \tag{2.15}$$

where $A=\sqrt{1-\gamma_1}\sqrt{1-\gamma_2}\sqrt{1-\gamma_3}\sqrt{1-\gamma_4}\sqrt{1-\kappa_1}$.

The output power of light propagation through the third NRR is

$$\frac{P_{t3}}{P_{in}}=\left|\frac{E_{t3}}{E_{in}}\right|^2. \tag{2.16}$$

When light propagation through the second 3dB, upper and lower MZI arms that on–off keying (OOK) or DPSK are controlled the optical pump in each NRR that yield

$$\begin{pmatrix} E_{out\_1}(On) \\ E_{out\_2}(Off) \end{pmatrix} = \sqrt{1-\gamma_5}\begin{pmatrix} \sqrt{1-\kappa_5} & j\sqrt{\kappa_5} \\ j\sqrt{\kappa_5} & \sqrt{1-\kappa_5} \end{pmatrix}\begin{pmatrix} E_{T3} \\ E_{22} \end{pmatrix}. \quad (2.17)$$

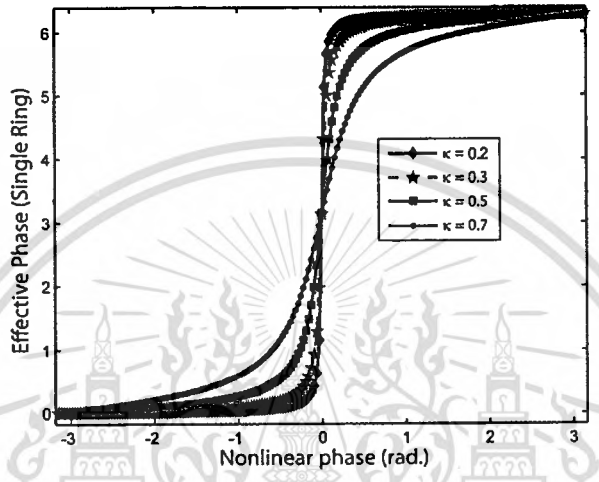

(a) Single NRR

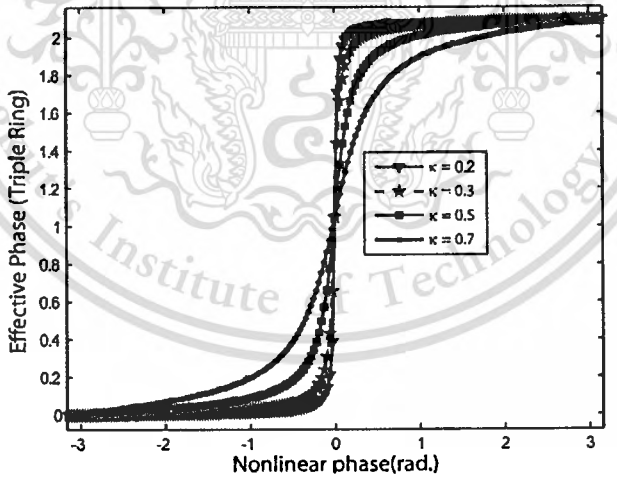

(b) Triple NRR

Figure 2.3 Simulation results of effective phase, where (a) single NRR vs. nonlinear phase (b) triple NRR vs. nonlinear phase. ($\alpha = 0.5dBmm^{-1}$, $\gamma = 0.1$, $n_2 = 2.2\times10^{-13}\ m^2/W$, $n_0 = 3.34$, $\lambda = 1.55\mu m$, $\beta = 0$)

For phase shaped binary transmission (PSBT), we generated input light pulse through NRRs that the difference phase shift is equal to π, as shown in figure 2.3.

In figure 2.3, shows variation of the effective phase due to nonlinear phase $\left(\phi_{NL} = (\omega_0/C)n_2(2\pi R_i)|E_{Ri}|^2\right)$, we assumed that $\beta = 0$, realize β is not equal to zero as shown in next section. In this curve the coupling coefficient is changed as parameter and with decrease of the coupling coefficient the slope of variation, we found that the effective phase of all–optical PSBT generation is fasted when the coupling coefficient of NRRs fixed at 0.2. So, with the small coupling coefficients very fast switching on-off power can be obtained and in our case only PSBT is necessary for on–off keying (OOK) in each NRR.

2.2 Dark–Bright Soliton Conversion

Optical solitons can naturally be divided into classes of dark and bright solitons. Specific, a dark soliton exhibits an interesting and remarkable behavior, when it is transmitted into an optical transmission system. It has the advantage of signal security, when the ambiguity of signal detection becomes a problem of the un–required users. Recently, Sarapat et al [41] have shown that the conversion of a dark soliton into a bright soliton can be realized using an add/drop filter. Here the secured signals in the transmission are retrieved using a suitable an add/drop filter that is connected to the transmission line. The other promising application of a dark soliton signal is confirmed by using the large guard band of two different frequencies which can be achieved by using a dark soliton generation scheme and trapping a dark soliton pulse within a nano ring resonator [42, 43]. Furthermore, the dark soliton pulse shows a more stable behavior than the bright solitons with respect to the perturbations such as amplifier noise, fiber losses, and intra–pulse stimulated Raman scattering [25]. It is found that the dark soliton pulses propagation in a lossy fiber, spreads in time at approximately half the rate of bright solitons. Heidari et al [44] have shown that the multichannel

wavelength conversion using three different types of dispersion profiles along the optical fibers. The dark solitons trapped in add/drop system is realized, therefore, optical tweezers appearance relation between scattering and gradient force of light propagation. Yuan et al [45] have shown an abruptly tapered twin–core fiber optical tweezers, by using two-beam combination technique and found that a strong enough gradient forces well tapered twin–core fiber optical tweezers. Optical tweezers were also characterized in terms of the optical potential well by measuring the displacement of trapped particles experiencing a viscous drag at a fluid flow below the critical velocity [46]. We are looking for a stationary dark soliton pulse, which is introduced into the multistage microring resonators as shown in Figure 2.4. The input optical field (E_{in}) of the dark soliton pulse input is given by [25, 47]

$$E_{in}(t) = A\tanh\left[\frac{T}{T_0}\right]\exp\left[\left(\frac{z}{2L_D}\right) - i\omega_0 t\right] \tag{2.18}$$

where A and z are the optical field amplitude and propagation distance, respectively. T is a soliton pulse propagation time in a frame moving at the group velocity, $T = t - \beta_1 * z$, where β_1 and β_2 are the coefficients of the linear and second–order terms of Taylor expansion of the propagation constant. $L_D = T_0^2/|\beta_2|$ is the dispersion length of the soliton pulse. T_0 in equation is a soliton pulse propagation time at initial input (or soliton pulse width), where t is the soliton phase shift time, and the frequency shift of the soliton is ω_0. This solution describes a pulse that keeps its temporal width invariance as it propagates, and thus is called a temporal soliton. When a soliton of peak intensity $\left(\left|\beta_2/\Gamma T_0^2\right|\right)$ is given, then T_0 is known. For the soliton pulse in the microring device, a balance should be achieved between the dispersion length (L_D) and the nonlinear length ($L_{NL} = 1/\Gamma\phi_{NL}$), where $\Gamma = n_2 * k_0$, is the length scale over which dispersive or nonlinear effects makes the beam become wider or narrower. For a soliton pulse, there is a balance between dispersion and nonlinear lengths. Hence $L_D = L_{NL}$.

When light propagates within the nonlinear medium, the refractive index (n) of light within the medium is given by

$$n = n_0 + n_2 I = n_0 + \frac{n_2}{A_{eff}} P, \tag{2.19}$$

where n_0 and n_2 are the linear and nonlinear refractive indexes, respectively. I and P are the optical intensity and optical power, respectively. The effective mode core area of the device is given by A_{eff}. For the microring resonator (MRR) and nanoring resonator (NRR), the effective mode core areas range from 0.50 to 0.10 μm^2 [48, 49]. When a soliton pulse is input and propagated within a MRR, as shown in Figure 2.4, which consists of a series MRRs. The resonant output is formed, thus, the normalized output of the light field is the ratio between the output and input fields [$E_{out}(t)$ and $E_{in}(t)$] in each roundtrip, which is given by [41]

$$\left|\frac{E_{out}(t)}{E_{in}(t)}\right|^2 = (1-\gamma)\left[1 - \frac{\left(1-(1-\gamma)x^2\right)\kappa}{\left(1-x\sqrt{1-\gamma}\sqrt{1-\kappa}\right)+4x\sqrt{1-\gamma}\sqrt{1-\kappa}\sin^2\left(\frac{\phi}{2}\right)}\right] \tag{2.20}$$

The close form of Equation (2.20) indicates that a ring resonator in this particular case is very similar to a Fabry–Perot cavity, which has an input and output mirror with a field reflectivity, $(1 - K)$, and a fully reflecting mirror. K is the coupling coefficient, and $x = \exp(-\alpha L/2)$ represents a roundtrip loss coefficient, $\phi_0 = kLn_0$ and $\phi_{NL} = kLn_2|E_{in}|^2$ are the linear and nonlinear phase shifts, $k = 2\pi/\lambda$ is the wave propagation number in a vacuum, where L and α are waveguide length and linear absorption coefficient, respectively. In this work, the iterative method is introduced to obtain the results as shown in Equation (2.20), and similarly, when the output field is connected and input into the other ring resonators.

To retrieve the signals from the chaotic noise, we propose to use the add/drop device with the appropriate parameters. This is given in the following details. The optical circuits of ring-resonator add/drop filters for the throughput and drop port can be given by Equations (2.21) and (2.22), respectively [41].

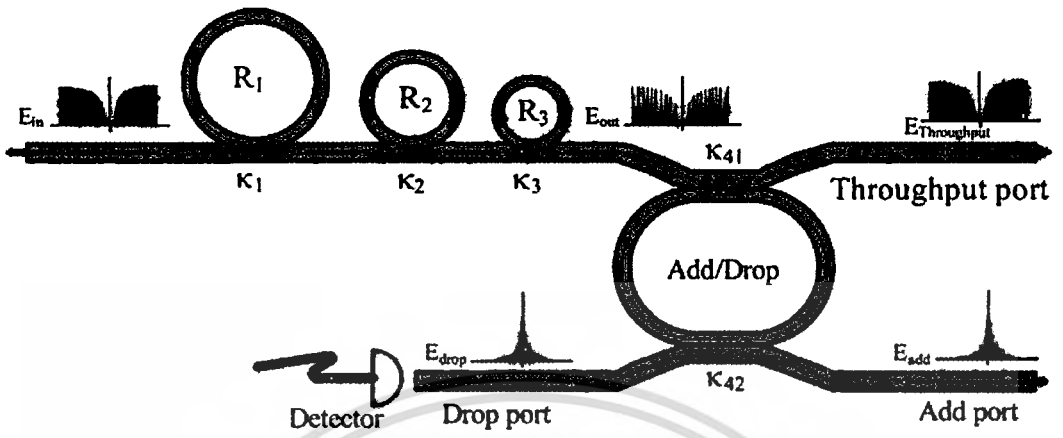

Figure 2.4 Schematic of a dark–bright soliton conversion system, where R_s is the ring radii, κ_s is the coupling coefficient, and κ_{41} and κ_{42} are the add/drop coupling coefficients.

$$\left|\frac{E_t}{E_{in}}\right|^2 = \frac{(1-\kappa_1)-2\sqrt{1-\kappa_1}\sqrt{1-\kappa_2}e^{-\frac{\alpha}{2}L}\cos(k_nL)+(1-\kappa_2)e^{-\alpha L}}{1+(1-\kappa_1)(1-\kappa_2)e^{-\alpha L}-2\sqrt{1-\kappa_1}\sqrt{1-\kappa_2}e^{-\frac{\alpha}{2}L}\cos(k_nL)} \tag{2.21}$$

and

$$\left|\frac{E_d}{E_{in}}\right|^2 = \frac{\kappa_1\kappa_2 e^{-\frac{\alpha}{2}L}}{1+(1-\kappa_1)(1-\kappa_2)e^{-\alpha L}-2\sqrt{1-\kappa_1}\sqrt{1-\kappa_2}e^{-\frac{\alpha}{2}L}\cos(k_nL)} \tag{2.22}$$

where E_t and E_d represent the optical fields of the throughput and drop ports, respectively. $\beta = kn_{eff}$ is the propagation constant, n_{eff} is the effective refractive index of the waveguide, and the circumference of the ring is $L = 2\pi R$ with R as the radius of the ring. In the following, new parameter is used for simplification with $\phi = \beta L$ as the phase constant. The chaotic noise cancellation can be managed by using the specific parameters of the add/drop device, and the required signals can be retrieved by the specific users. κ_1 and κ_2 are the coupling coefficient of the add/drop

filters, $k_n = 2\pi/\lambda$ is the wave propagation number for in a vacuum, and where the waveguide (ring resonator) loss is $\alpha = 0.5\ dBmm^{-1}$. The fractional coupler intensity loss is $\gamma = 0.1$. In the case of the add/drop device, the nonlinear refractive index is neglected.

Dark–bright soliton control has been investigated clearly by the authors in reference [41], where one of the advantages is that the dark soliton peak signal is always low level, which can be useful for secured signal communication in the transmission link. The other is formed when the high optical field is configured as an optical tweezer or potential well, which is available for atom/molecule trapping. Optical tweezers technique has become a powerful tool for manipulation of micrometer-sized particles in three spatial dimensions [50]. Initially, the useful static tweezer is recognized, and the dynamic tweezer is now realized in practical work. Typically, by using the continuous-wave (cw) lasers, the spatial control of atoms, beyond their trapping in stationary potentials, has been continuously gaining importance in investigations of ultra cold gases and in the application of atomic ensembles and single atoms for cavity quantum electrodynamics (QED) and quantum information studies. Recent progress includes the trapping and control of single atoms in dynamic potentials [51, 52], the sub–micron positioning of individual atoms with standing–wave potentials [53, 54], micro–structured and dynamic traps for Bose–Einstein condensates [55, 56, 57] and, as another example, the realization of chaotic dynamics in atom–optics "billiards" [58, 59, 60]. Recently, Schulz et al [61] have shown that the transfer of trapped atoms between two optical potentials could be performed. In this section, I present a novel system of the optical tweezers storage using a dark–bright soliton pulse propagating within an add/drop optical filter. The multiplexing signals with different wavelengths of the dark solitons are controlled and amplified within the system. The dynamic behaviors of dark–bright soliton interaction are analyzed and described. The storage signals are controlled and tuned to be an optical probe which is known as the optical tweezers. The optical tweezers storages are obtained by using the embedded nanoring resonators within the add/drop optical filter system. The controlled light pulses are added into the add port of the add/drop filter. By using the bright soliton input, the different in time of the first two dynamic wells of 1 ns is noted,

while the potential well stability is seen when the Gaussian pulse is input into the add port. In application, the optical tweezers can be stored and trapped light/atom, which can be formed the dynamic tweezers and tweezers memory.

Experimentally, the generated dark soliton pulse, for instance, with 50ns pulse width, and a maximum power of $0.65W$ is input into the dark-bright soliton conversion system, as shown in Figure 2.4. The suitable ring parameters are used, such as ring radii where $R_1=10.0\mu m$, $R_2=7.0\mu m$, and $R_3=5.0\mu m$. In order to make the system associate with the practical device [48, 49], whereas the selected parameters of the system are fixed to $\lambda_0=1.50\mu m$, $n_0=3.34$ (InGaAsP/InP). The effective core areas are $A_{eff}=0.50$, 0.25, and $0.10\ \mu m^2$ for a MRR and NRR, respectively. The waveguide and coupling loses are $\alpha=0.5dBmm^{-1}$ and $\gamma=0.1$, respectively, and the coupling coefficients κ_s of the MRR are ranged from 0.05 to 0.90. However, more parameters are used as shown in Figure 2.4. The nonlinear refractive index is $n_2=2.2\times10^{-13}\ m^2/W$. In this case, the waveguide loss used is $0.5\ dBmm^{-1}$. The input dark soliton pulse is chopped (sliced) into the smaller signals, where the filtering signals within the rings R_2 and R_3 are seen. We find that the output signals from R_3 are smaller than from R_1, which is more difficult to detect when it is used in the link. In fact, the multistage ring system is proposed due to the different core effective areas of the rings in the system, where the effective areas can be transferred from 0.50 to $0.10\mu m^2$ with some losses. The soliton signals in R_3 is entered in the add/drop filter, where the dark–bright soliton conversion can be performed by using Equations (9) and (10). Results obtained when a dark soliton pulse is input into a MRR and NRR system as shown in Figure 2.4. The add/drop filter is formed by using two couplers and a ring with radius (R_d) of $10\mu m$, the coupling constants (κ_{41} and κ_{42}) are the same values (0.50). When the add/drop filter is connected to the third ring (R_3), the dark–bright soliton conversion can be seen. The bright and dark solitons are detected by the through (throughput) and drop ports as shown in Figure 2.5(a) – (e), respectively.

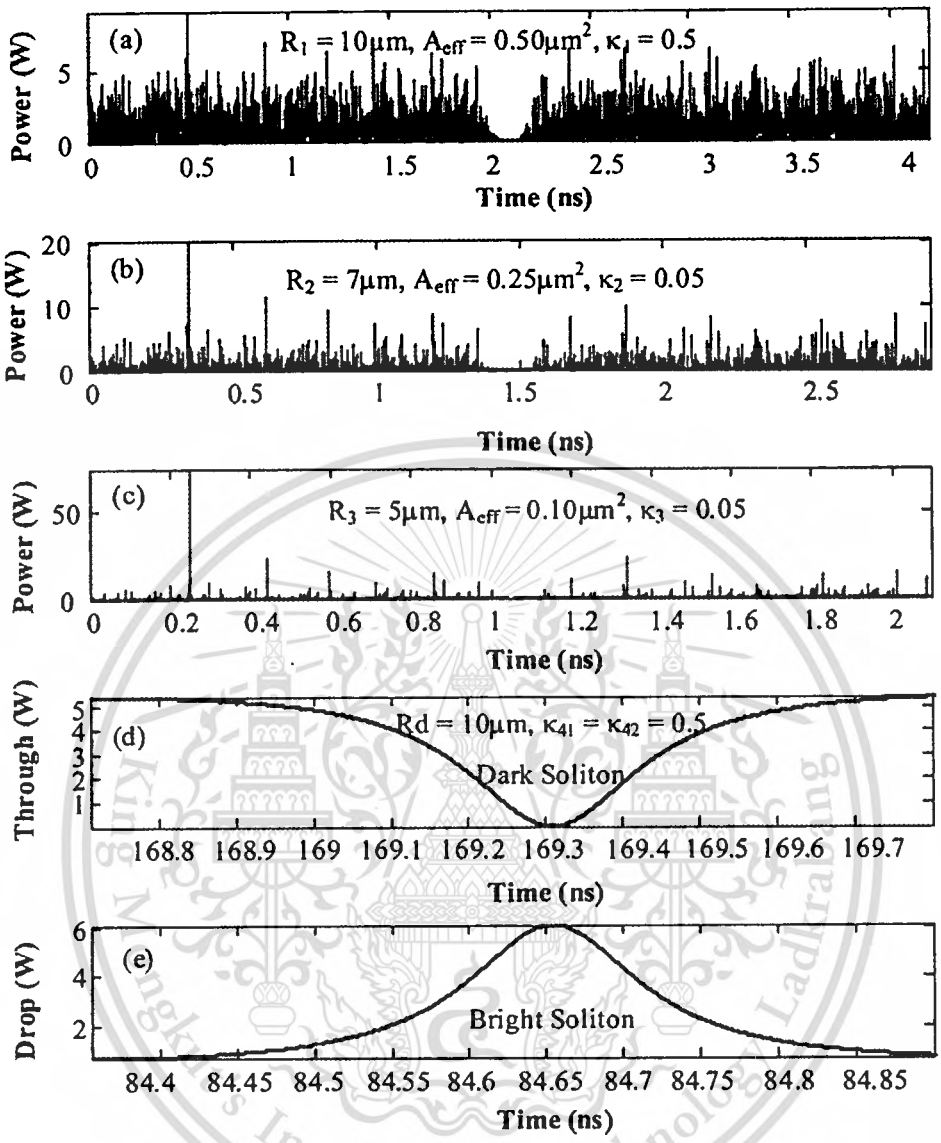

Figure 2.5. Results of the soliton signals within the ring resonator system, where (a) R_1, (b) R_2, (c) R_3, and (d) – (e) dark–bright solitons conversion at the add/drop filter. The input dark soliton power is 2W.

2.3 Dark–Bright Soliton Conversion in Add/Drop Filter

In operation, dark–bright soliton conversion using a ring resonator optical channel dropping filter (OCDF) is composed of two sets of coupled waveguides, as shown in Figure 2.6. The relative phase of the two output light signals after coupling into the optical coupler is $\pi/2$ before coupling into the ring and the input bus, respectively. This means that the signals coupled into the drop and through ports are acquired a phase of π with respect to the input port signal. In application, if we engineer the coupling coefficients appropriately, the field coupled into the through port on resonance would completely extinguish the resonant wavelength, and all power would be coupled into the drop port. I will show that this is possible later in this section.

$$E_{ra} = -j\kappa_1 E_i + \tau_1 E_{rd}, \tag{2.23}$$

$$E_{rb} = \exp(j\omega T/2)\exp(-\alpha L/4)E_{ra}, \tag{2.24}$$

$$E_{rc} = \tau_2 E_{rb} - j\kappa_2 E_a, \tag{2.25}$$

$$E_{rd} = \exp(j\omega T/2)\exp(-\alpha L/4)E_{rc}, \tag{2.26}$$

$$E_t = \tau_1 E_i - j\kappa_1 E_{rd}, \tag{2.27}$$

$$E_d = \tau_2 E_a - j\kappa_2 E_{rb}, \tag{2.28}$$

Where E_i is the input field, E_a is the add (control) field, E_t is the through field, E_d is the drop field, $E_{ra}...E_{rd}$ are the fields in the ring at points $a...d$, κ_1 is the field coupling coefficient between the input bus and ring, κ_2 is the field coupling coefficient between the ring and output bus, L is the circumference of the ring, T is the time taken for one round trip (roundtrip time), and α is

the power loss in the ring per unit length. We assume that this is the lossless coupling, i.e., $\tau_{1,2} = \sqrt{1-\kappa_{1,2}^2}$. $T = Ln_{eff}/c$.

The output power/intensities at the drop and through ports are given by

$$|E_d|^2 = \left| \frac{-\kappa_1\kappa_2 A_{1/2}\Phi_{1/2}}{1-\tau_1\tau_2 A\Phi} E_i + \frac{\tau_2 - \tau_1 A\Phi}{1-\tau_1\tau_2 A\Phi} E_a \right|^2 . \tag{2.29}$$

$$|E_t|^2 = \left| \frac{\tau_2 - \tau_1 A\Phi}{1-\tau_1\tau_2 A\Phi} E_i + \frac{-\kappa_1\kappa_2 A_{1/2}\Phi_{1/2}}{1-\tau_1\tau_2 A\Phi} E_a \right|^2 . \tag{2.30}$$

where $A_{1/2} = \exp(-\alpha L/4)$ (the half–round–trip amplitude), $A = A_{1/2}^2$, $\Phi_{1/2} = \exp(j\omega T/2)$ (the half–round–trip phase contribution), and $\Phi = \Phi_{1/2}^2$.

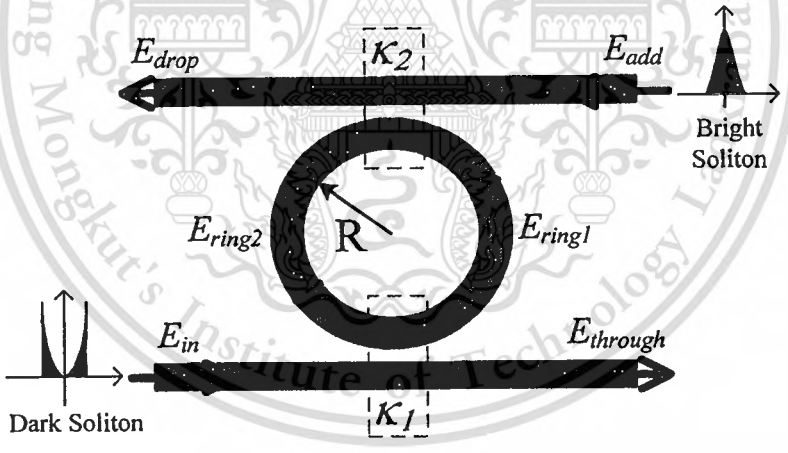

Figure 2.6 Sheme of dark–bright soliton conversion using a ring resonator optical channel dropping filter (OCDF).

The input and control fields at the input and add ports are formed by the dark–bright optical soliton as shown in Equations (31) – (32),

$$E_{in}(t) = E_0 \tanh\left[\frac{T}{T_0}\right] \exp\left[\left(\frac{z}{2L_D}\right) - i\omega_0 t\right] \tag{2.31}$$

$$E_{in}(t) = E_0 \sec h\left[\frac{T}{T_0}\right]\exp\left[\left(\frac{z}{2L_D}\right) - i\omega_0 t\right] \tag{2.32}$$

where E_0 and z are the optical field amplitude and propagation distance, respectively. $T = t - \beta_1 z$, where β_1 and β_2 are the coefficients of the linear and second–order terms of Taylor expansion of the propagation constant. $L_D = T_0^2/|\beta_2|$ is the dispersion length of the soliton pulse. T_0 in equation is a soliton pulse propagation time at initial input (or soliton pulse width), where t is the soliton phase shift time, and the frequency shift of the soliton is ω_0.

When the optical field is entered into the nanoring resonator as shown in Figure 2.7, where the coupling coefficient ratio K_1: K_2 are *50:50, 90:10, 10: 90.* By using (a) dark soliton is input into input and control ports, (b) dark and bright soliton are used for input and control signals, (c) bright and dark soliton are used for input and control signals, and (d) bright soliton is used for input and control signals. The ring radii $R_{ad} = 5\mu m$, $A_{eff} = 0.25\mu m^2$, $n_{eff} = 3.14$ (for InGaAsP/InP), $\alpha = 5dB/mm$, $\gamma = 0.1$, $\lambda_0 = 1.51\ \mu m$.

In application, the dynamic optical tweezers is occurred, when we added bright soliton input at the add port with shown in Figure 2.8, the parameters of system are set the same as the previous section. The bright soliton was generated at the central wavelength $\lambda_0 = 1.5\mu m$, when the bright soliton propagating into the add/drop system, the occurrence of dark–bright soliton collision in add/drop system is shown in Figure 2.8(a) – (d) and Figure 2.9(a) – (d).

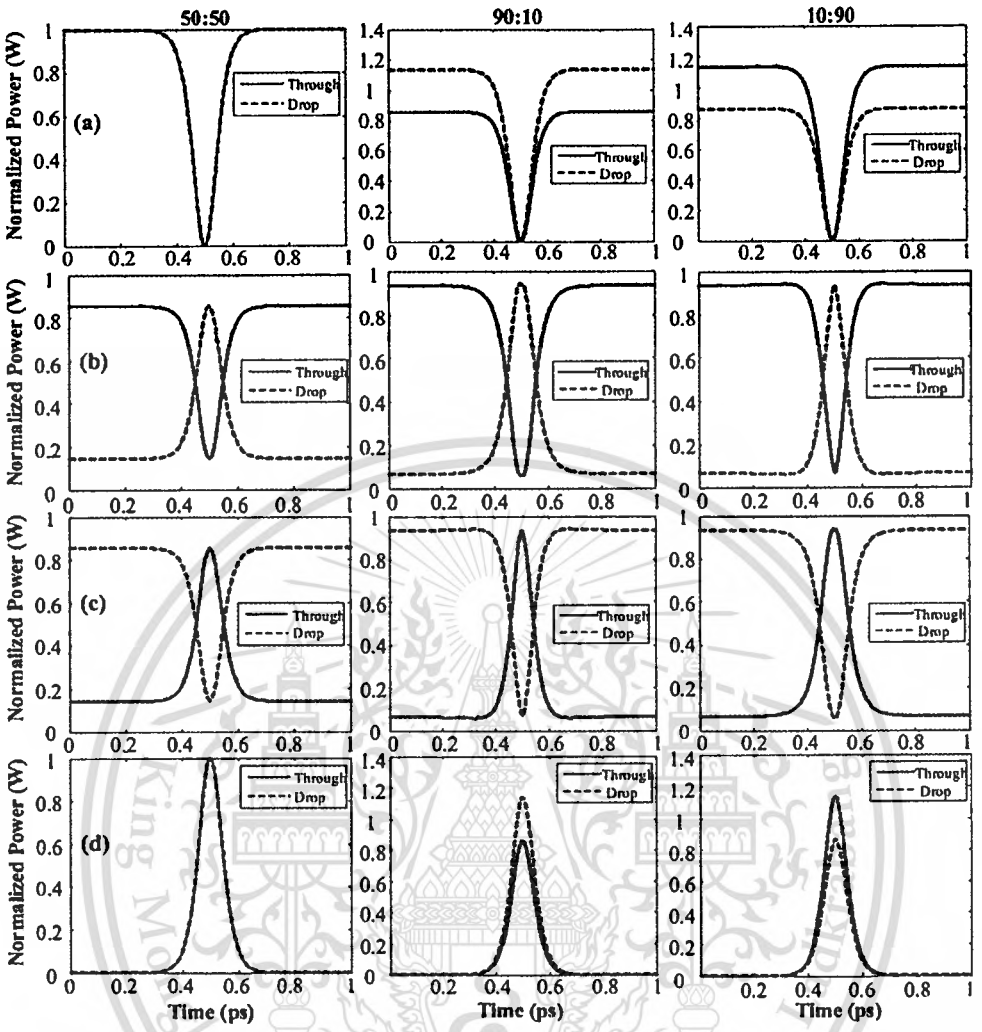

Figure 2.7 Dark–bright soliton conversion results using a ring resonator optical channel dropping filter (OCDF) [62].

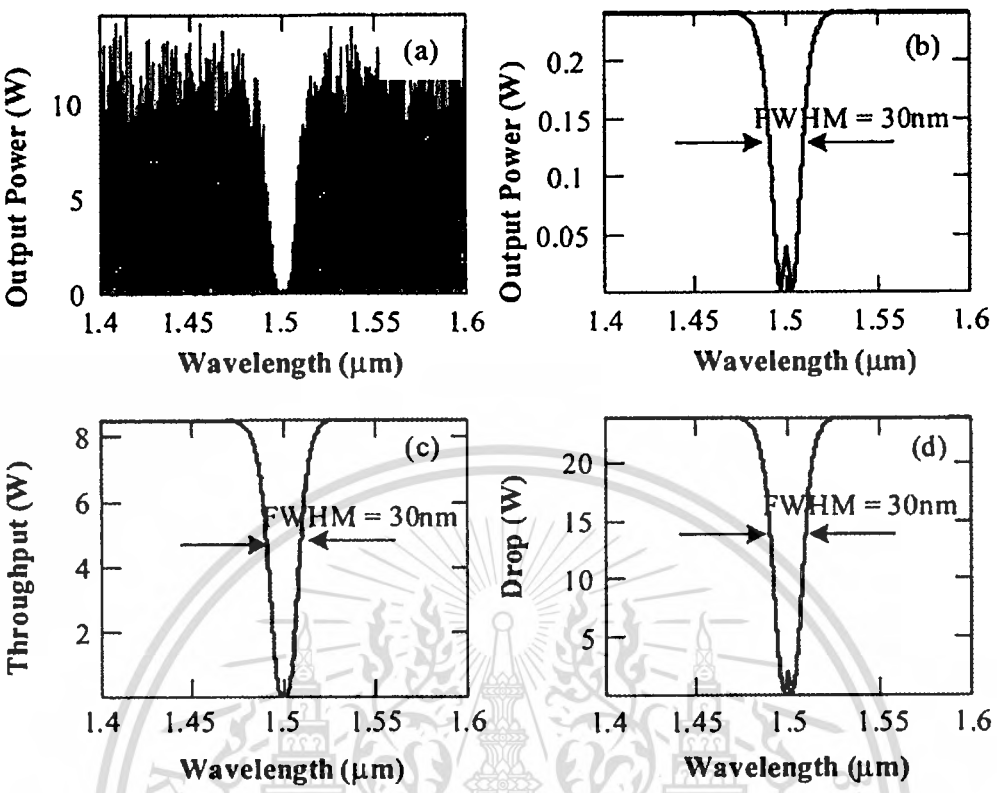

Figure 2.8 The dynamic optical tweezers output within the add/drop filter, when the bright soliton input with the central wavelength $\lambda_0 = 1.5\mu m$, where (a) add/drop signal, (b) dark–bright soliton collision, (c) optical tweezers at throughput port, and (d) optical tweezers at drop port.

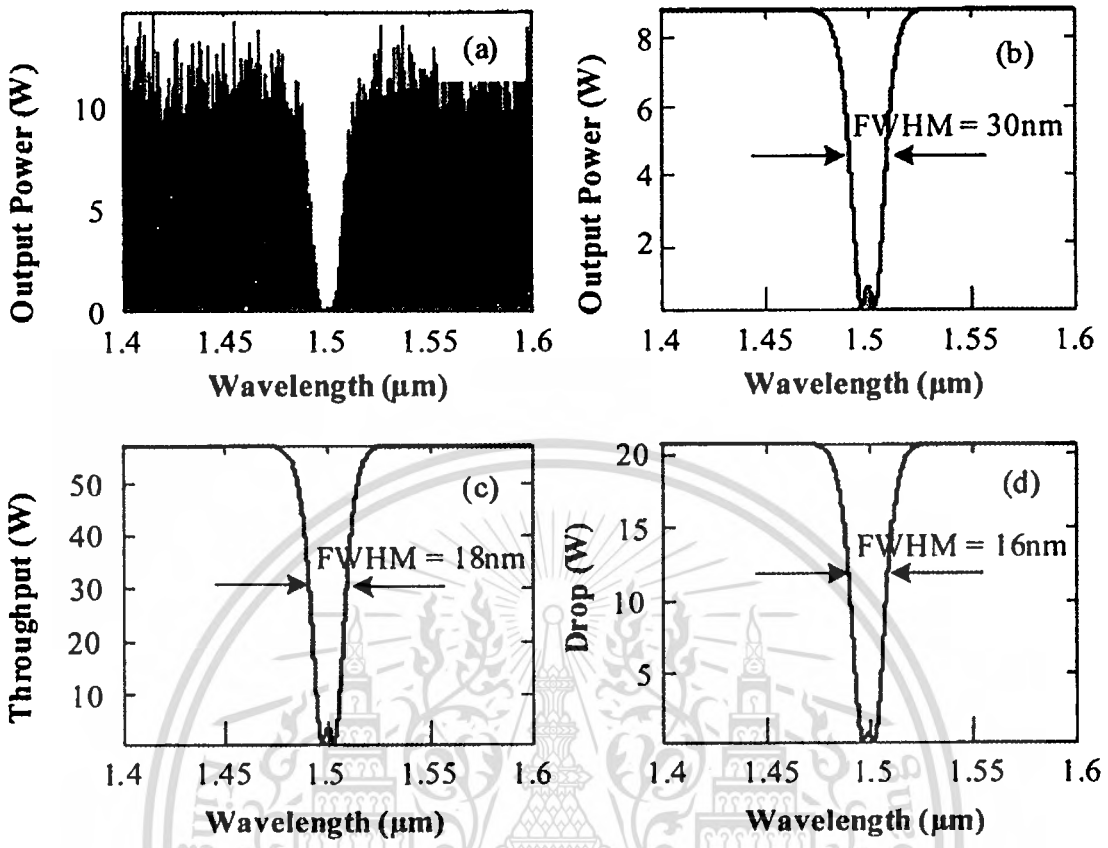

Figure 2.9 The tuned dynamic optical tweezers output within the add/drop filter, when the bright soliton input with the central wavelength $\lambda_0 = 1.5\mu m$, where (a) the add/drop signal, (b) dark–bright soliton collision, (c) optical tweezers at throughput port, and (d) optical tweezers at drop port.

CHAPTER 3

OOK generation based on MZI incorporating a pumped nonlinear ring resonators system

In this chapter present an interesting result of nonlinear light pulse propagation within a Mach–Zehnder Inteferometer (MZI) which can be used to extend the existed on–off keying (OOK) techniques. The goal of this chapter is OOK generation based on MZI incorporating a pumped nonlinear ring resonators system. First analyze the principles of a phase modulation scheme using MZI incorporating the triple nonlinear ring resonators, which can be fabricated and used in practical communications. After that, focus on the recent modulation schemes, where the all–optical on off keying and the phase shift control for phase shaped binary transmission (PSBT) are discussed in details. The novelty of this work is that the nonlinear ring resonators are used incorporating a MZI, where the extended switching generation can be achieved and seen.

3.1 Introduction

Today, most of the optical communication links use the well known modulation format called OOK (On–Off Keying)[1 – 9], which is due to the increasing in bit rates, power and number of DWDM (Dense Wavelength Division Multiplexing) channels, where the OOK format can reach the communication requirement. However, the various modulation schemes have already been used in the electrical domain during last decade, but they have not been applied in optical schemes. Recently the use of new modulation formats in optical communications has been considered and compared for increasing the tolerance of the optical link to impairments such as chromatic dispersion, PMD (Polarization mode dispersion) or nonlinearity (Kerr Effect) [10]. Among the various modulation formats, I present here the differential phase shift keying (DPSK) and the phase shaped binary transmission (PSBT) schemes, whereas DPSK presents a better

robustness to optical nonlinearities than the classical OOK, particularly for the cross phase modulation (XPM) in DWDM systems [3, 9, 11]. Moreover, it has also been shown that DPSK format has better performances due to PMD degradations than the classical OOK [9, 11]. The disadvantage of the DPSK is that a direct detection (DD) at the end of the optical link is not possible, since DPSK is a phase modulation. Thus, an interferometric demodulation stage must be inserted in front of the photo-detector. This stage is an "Add and Delay" structure, which is composed by a MZI [9, 11 – 15].

In this chapter, first describe the principles of light propagation in the proposed system, where the nonlinear behavior of light within the nonlinear ring resonators (NRRs) can be used to analyze for PSBT modulation. After that, the MZI structure is detailed. However, the nonlinear ring resonator has been used [16 – 19] for phase shifted generate by couple to one arm of a MZI [16 – 17]. In this structure, one arm presents an optical delay line equal to the bit duration. This MZI converts an optical DPSK to an intensity–modulated (IM) signal, which is followed by a DD. The PSBT format is encoded from a DPSK: first a DPSK signal is generated and after that a MZI structure converts the DPSK to be an intensity-modulated signal: the PSBT. MZI characteristics for the two applications are slightly different, as we will see in the next sections. The novelty of this work is that the nonlinear light pulses generated by using the triple nonlinear ring resonators in one arm of a Mach–Zehnder interferometer can be used to enhance (amplify) the light pulse output signals, where the nonlinear outputs are generated by using the nonlinear coefficient refractive index $n_2 = 2.2\times10^{-13}\ m^2/W$.

3.2 Principles of modulation

Figure 3.1 shows the proposal for on–off keying model using nonlinear index of refraction in three nonlinear ringresonator coupled to one arm of Mach–Zehnder interferometer. In this figure there are similar NRRs with the field–dependent absorption and index of refraction coefficients.

When the input field, E_{in}, passes through 3dB coupler with coupling coefficient ratio, K_1, 50:50, then light is split into two ways, which can be expressed as

$$E_{11} = \sqrt{1-\gamma_1}\sqrt{1-\kappa_1}E_{in}, \tag{3.1}$$

$$E_{21} = j\sqrt{1-\gamma_1}\sqrt{\kappa_1}E_{in}, \tag{3.2}$$

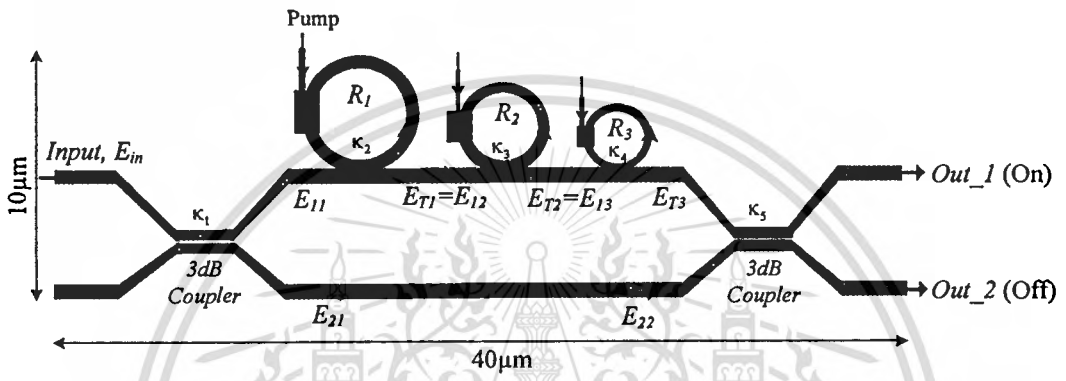

Figure 3.1 Schematic diagram of OOK system, system size is $10 \times 40 \mu m^2$.

According to the linear coupling theory, the following relations can connect input–output fields for each nonlinear ring resonators (NRRs) as shown in figure 3.2, which can be expressed by [17]

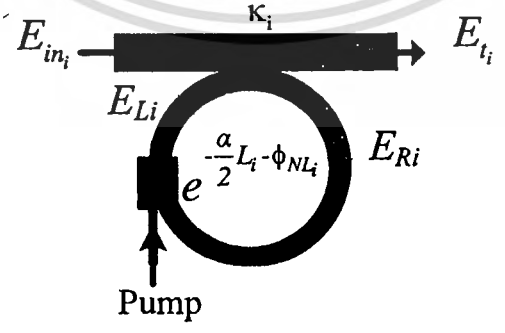

Figure 3.2 Schematic diagram of single NRR (i = 2, 3, 4).

$$E_{Ri} = \sqrt{1-\gamma_i}\sqrt{1-\kappa_i}E_{Li} + j\sqrt{1-\gamma_i}\sqrt{\kappa_i}E_{in_i}, \tag{3.3}$$

$$E_{t_i} = \sqrt{1-\gamma_i}\sqrt{1-\kappa_i}E_{in_i} + j\sqrt{1-\gamma_i}\sqrt{\kappa_i}E_{Li}, \tag{3.4}$$

where γ_i and κ_i are the coupler loss and coupling coefficient in each NRR, respectively. Since the NRR length and the nonlinear index of refraction are small, therefore, the nonlinear Schrodinger equation (NLS) can be used to solve light propagation through the NRRs, the solution is given by [17]

$$E_{Li} = E_{Ri}\exp\left(-\frac{\alpha}{2}L_i - \gamma_{NL_i}\left|E_{Ri}\right|^2 L_i\right). \tag{3.5}$$

where α, $L_i = 2\pi R_i$ and γ_{NL_i} are the NRR loss, NRR length (R_i is ring radius) and the nonlinear coefficient including the nonlinear index of refraction and two–photon absorption phenomenon, respectively. By using the basic concepts in nonlinear optics, the following relation can be used for the above mentioned, the nonlinear coefficient is given by

$$\gamma_{NL_i} = \frac{\beta}{2} - j\frac{\omega_0}{c}n_2 \tag{3.6}$$

where β, ω_0, C and n_2 are the two–photon absorption coefficient, incident light frequency, speed of light in free space and the nonlinear index of refraction coefficient, respectively. The following relation describes the nonlinear phenomenon in the NRRs as

$$\begin{aligned} \tilde{\alpha} &= \alpha + \beta\left|E\right|^2, \\ \tilde{n} &= n + n_2\left|E\right|^2, \end{aligned} \tag{3.7}$$

where both of the absorption coefficient and index of refraction includes linear and nonlinear parts and the following relations can be used for obtaining these variables in terms of the optical third order susceptibility as

$$n_2 = \frac{3}{8n}\mathrm{Re}\left[\chi^{(3)}\right],$$

$$\beta = \frac{3\omega_0}{4nC}\mathrm{Im}\left[\chi^{(3)}\right]. \tag{3.8}$$

Using Eqs. (3.3) – (3.5) and some mathematical manipulations, the following transmission functions can be obtained for each NRRs as

$$T = \frac{E_{t_i}}{E_{in_i}} = \sqrt{1-\gamma_i}\sqrt{1-\kappa_i} - \frac{\kappa_i(1-\gamma_i)\exp\left(-\frac{\alpha}{2}L_i - \phi_{NL_i}\right)}{1-\sqrt{1-\gamma_i}\sqrt{1-\kappa_i}\exp\left(-\frac{\alpha}{2}L_i - \phi_{NL_i}\right)}. \tag{3.9}$$

where $\phi_{NL_i} = \gamma_{NL_i} L_i |E_{Ri}|^2$ is defined as a nonlinear phase shift.

For the obtained result in Eq. (3.9), the phase difference (effective phase from single NRR) can be found as follows:

$$\phi_{eff} = \phi_i = \tan^{-1}\left[\frac{-\kappa_i(1-\gamma_i)e^{-1/2\left(\alpha+\beta|E_{Ri}|^2\right)L_i} \times \sin\left((\omega_0/C)n_2 L_i |E_{Ri}|^2\right)}{A+B+D}\right], \tag{3.10}$$

where $A = (2-\kappa_i)(1-\gamma_i)e^{-1/2\left(\alpha+\beta|E_{Ri}|^2\right)L_i}\cos\left((\omega_0/C)n_2 L_i |E_{Ri}|^2\right)$, $B = \sqrt{(1-\kappa_i)(1-\gamma_i)}$ and $D = (1-\gamma_i)\sqrt{(1-\kappa_i)(1-\gamma_i)}e^{-\left(\alpha+\beta|E_{Ri}|^2\right)L_i}$.

The obtained result can be simplified to the following formula, which is assumed by $\gamma_i = \alpha = \beta = 0$.

$$\phi_{eff} = \phi_i = \tan^{-1}\left[\frac{-\kappa_i \sin\left(\frac{\omega_0}{C}n_2 L_i |E_{Ri}|^2\right)}{2\sqrt{1-\kappa_i} - (2-\kappa_i)\cos\left(\frac{\omega_0}{C}n_2 L_i |E_{Ri}|^2\right)}\right]. \tag{3.11}$$

In real system $\gamma_i, \alpha,$ and β are not be zero as shown in section 3, $\alpha = 0.5 dBmm^{-1}$, $\gamma = 0.1$ and $\beta = 2 \times 10^{-11}$, respectively.

And, the output power at light propagation through the first NRR is given by

$$\frac{P_{t1}}{P_{in}} = \left|\frac{E_{t1}}{E_{in}}\right|^2. \tag{3.12}$$

The electric field of light propagation through the second NRR is given by

$$\frac{E_{t2}}{E_{in}}=\frac{\sqrt{1-\gamma_1}\sqrt{1-\gamma_2}\sqrt{1-\gamma_3}\sqrt{1-\kappa_1}\begin{pmatrix}\sqrt{1-\kappa_2}\sqrt{1-\kappa_3}-\sqrt{1-\gamma_2}\sqrt{1-\kappa_3}e^{-\frac{\alpha}{2}L_1-\phi_{NL,1}}\\-\sqrt{1-\gamma_3}\sqrt{1-\kappa_2}\,e^{-\frac{\alpha}{2}L_2-\phi_{NL,2}}\\+\sqrt{1-\gamma_2}\sqrt{1-\gamma_3}\,e^{-\frac{\alpha}{2}(L_1+L_2)-(\phi_{NL,1}+\phi_{NL,2})}\end{pmatrix}}{\begin{pmatrix}1+\sqrt{1-\gamma_2}\sqrt{1-\kappa_2}\,e^{-\frac{\alpha}{2}L_1-\phi_{NL,1}}-\sqrt{1-\gamma_3}\sqrt{1-\kappa_3}\,e^{-\frac{\alpha}{2}L_2-\phi_{NL,2}}\\+\sqrt{1-\gamma_2}\sqrt{1-\gamma_3}\sqrt{1-\kappa_2}\sqrt{1-\kappa_3}\,e^{-\frac{\alpha}{2}(L_1+L_2)-(\phi_{NL,1}+\phi_{NL,2})}\end{pmatrix}}, \quad (3.13)$$

where $\sqrt{1-\gamma_1}$, $\sqrt{1-\gamma_2}$, $\sqrt{1-\gamma_3}$, $\sqrt{1-\gamma_4}$ and $\sqrt{1-\gamma_5}$ are coupler losses in each coupler and $\sqrt{1-\kappa_1}$, $\sqrt{1-\kappa_2}$, $\sqrt{1-\kappa_3}$, $\sqrt{1-\kappa_4}$ and $\sqrt{1-\kappa_5}$ are coupler separates in each coupler, respectively.

The output power of light propagation through the second NRR is given by

$$\frac{P_{t2}}{P_{in}}=\left|\frac{E_{t2}}{E_{in}}\right|^2. \quad (3.14)$$

The electric field of light propagation through third NRR the relation input–output field is

$$\frac{E_{t3}}{E_{in}}=\frac{A\begin{pmatrix}\sqrt{1-\kappa_2}\sqrt{1-\kappa_3}\sqrt{1-\kappa_4}\\ -\sqrt{1-\kappa_3}\sqrt{1-\kappa_4}e^{-\frac{\alpha}{2}L_1-\phi_{NL,1}}\\ -\sqrt{1-\kappa_2}\sqrt{1-\kappa_4}e^{-\frac{\alpha}{2}L_2-\phi_{NL,2}}\\ +\sqrt{1-\kappa_4}e^{-\frac{\alpha}{2}(L_1+L_2)-(\phi_{NL,1}+\phi_{NL,2})}\\ -\sqrt{1-\kappa_2}\sqrt{1-\kappa_3}e^{-\frac{\alpha}{2}L_3-\phi_{NL,3}}\\ +\sqrt{1-\kappa_3}e^{-\frac{\alpha}{2}(L_1+L_3)-(\phi_{NL,1}+\phi_{NL,3})}\\ +\sqrt{1-\kappa_2}e^{-\frac{\alpha}{2}(L_2+L_3)-(\phi_{NL,2}+\phi_{NL,3})}\\ +\sqrt{1-\kappa_3}\sqrt{1-\kappa_4}e^{-\frac{\alpha}{2}(L_1+L_2+L_3)-(\phi_{NL,1}+\phi_{NL,2}+\phi_{NL,3})}\end{pmatrix}}{\begin{pmatrix}1+\sqrt{1-\gamma_2}\sqrt{1-\kappa_2}e^{-\frac{\alpha}{2}L_1-\phi_{NL,1}}\\ -\sqrt{1-\gamma_3}\sqrt{1-\kappa_3}e^{-\frac{\alpha}{2}L_2-\phi_{NL,2}}-\sqrt{1-\gamma_4}\sqrt{1-\kappa_4}e^{-\frac{\alpha}{2}L_3-\phi_{NL,3}}\\ +\sqrt{1-\gamma_2}\sqrt{1-\gamma_3}\sqrt{1-\kappa_2}\sqrt{1-\kappa_3}e^{-\frac{\alpha}{2}(L_1+L_2)-(\phi_{NL,1}+\phi_{NL,2})}\\ +\sqrt{1-\gamma_3}\sqrt{1-\gamma_4}\sqrt{1-\kappa_3}\sqrt{1-\kappa_4}e^{-\frac{\alpha}{2}(L_2+L_3)-(\phi_{NL,2}+\phi_{NL,3})}\\ -\sqrt{1-\gamma_2}\sqrt{1-\gamma_3}\sqrt{1-\gamma_4}\sqrt{1-\kappa_2}\sqrt{1-\kappa_3}\sqrt{1-\kappa_4}\\ \times e^{-\frac{\alpha}{2}(L_1+L_2+L_3)-(\phi_{NL,1}+\phi_{NL,2}+\phi_{NL,3})}\end{pmatrix}}, \tag{3.15}$$

where $A=\sqrt{1-\gamma_1}\sqrt{1-\gamma_2}\sqrt{1-\gamma_3}\sqrt{1-\gamma_4}\sqrt{1-\kappa_1}$.

The output power of light propagation through the third NRR is

$$\frac{P_{t3}}{P_{in}}=\left|\frac{E_{t3}}{E_{in}}\right|^2. \tag{3.16}$$

When light propagation through the second 3dB, upper and lower MZI arms that on–off keying (OOK) or DPSK are controlled the optical pump in each NRR that yield

$$\begin{pmatrix}E_{out\_1}(On)\\ E_{out\_2}(Off)\end{pmatrix}=\sqrt{1-\gamma_5}\begin{pmatrix}\sqrt{1-\kappa_5} & j\sqrt{\kappa_5}\\ j\sqrt{\kappa_5} & \sqrt{1-\kappa_5}\end{pmatrix}\begin{pmatrix}E_{T3}\\ E_{22}\end{pmatrix}. \tag{3.17}$$

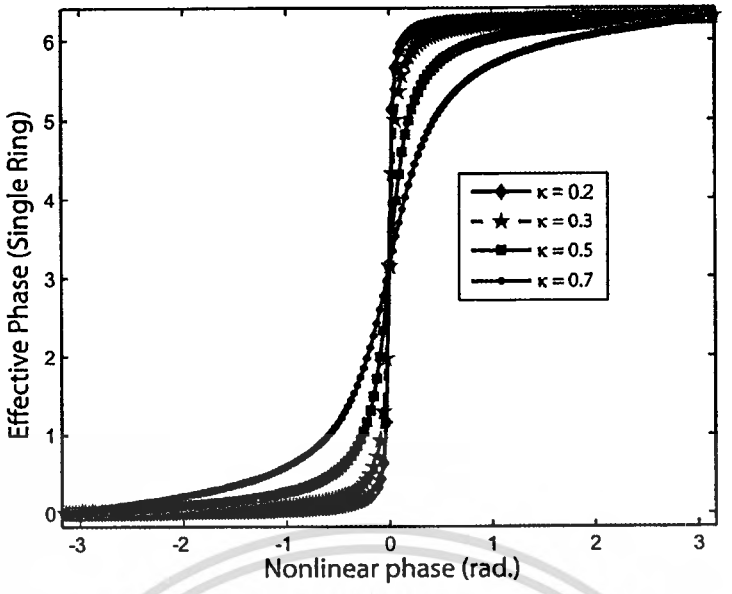

(a) Single NRR

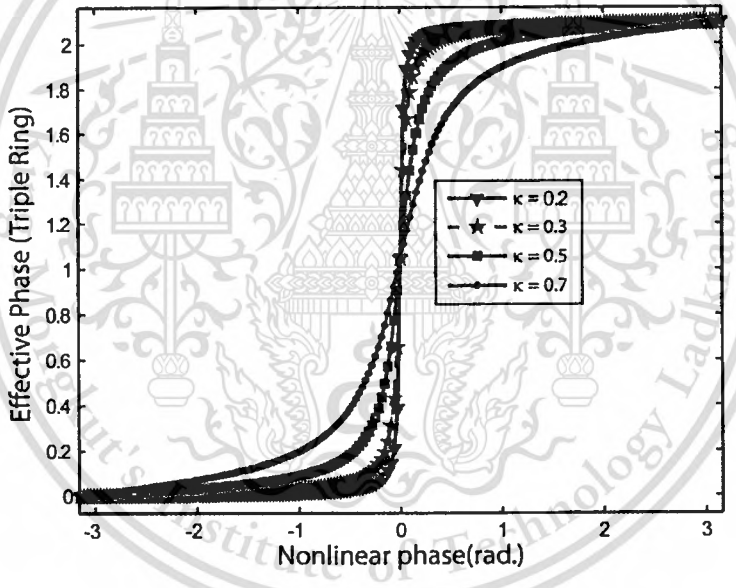

(b) Triple NRR

Figure 3.3 Simulation results of effective phase, where (a) single NRR vs. nonlinear phase (b) triple NRR vs. nonlinear phase. *(α = 0.5dBmm^{-1}, γ=0.1, n_2 = 2.2×10^{-13} m^2/W, n_0 = 3.34, λ = 1.55μm, β = 0)*

For phase shaped binary transmission (PSBT), we generated input light pulse through NRRs that the difference phase shift is equal to π, as shown in Figure 3.3.

In Figure 3.3, shows variation of the effective phase due to nonlinear phase $\left(\phi_{NL} = (\omega_0/C)n_2(2\pi R_i)|E_{Ri}|^2\right)$, we assumed that $\beta = 0$, realize β is not equal to zero as shown in next section. In this curve the coupling coefficient is changed as parameter and with decrease of the coupling coefficient the slope of variation, I found that the effective phase of all–optical PSBT generation is fasted when the coupling coefficient of NRRs fixed at 0.2. So, with the small coupling coefficients very fast switching on–off power can be obtained and in our case only PSBT is necessary for on–off keying (OOK) in each NRR.

3.3 OOK Generation

In operation, all–optical OOK generated maximum power of *3mW* Gaussian modulated CW is input into the OOK system, as shown in Figure 3.1. The suitable NRRs parameters are used, such as NRR radii where $R_1 = 1.5\mu m$, $R_2 = 1.0\mu m$ *and* $R_3 = 0.775\mu m$. In order to make the system associate with the practical device [62, 63], the selected parameters of the system are fixed to λ_0=*1.55*μm and *1.31*μm, n_0=*3.34* (GaInAsP/InP waveguide). The effective core areas are A_{eff} = *0.10* μm^2 for NRRs. The waveguide and coupling loses are α = 0.5dBmm^{-1} and γ = *0.1*, respectively, and the coupling coefficients K_i of the NRRs fixed *0.5*and $\beta = 2 \times 10^{-11}$ [17]. As for the numerical simulation of all–optical OOK, PSBT and DPSK, all our numerical work has been carried out by using commercially available simulation software-the OptiFDTD simulation package [64] which is based explicitly on the model described above [40]. However, more parameters are used as shown in Figure 3.1. The nonlinear refractive index is $n_2 = 2.2\times10^{-13}$ m^2/W. In this case, the waveguide loss used is 0.5 dBmm^{-1} and the size of the waveguide desired system is *10* $\times$ *40* μm^2. Numerical results are generated at input power of *3mW* Gaussian modulated CW at wavelength center λ_0 = *1.55*μm with time offset 4 $\times$ 10^{-14}s, half width 1.5 $\times$

10^{-14}s. All numerical work has been carried out by using commercially available simulation software-the OptiFDTD simulation package.

In Figure 3.4, the numerical simulation OOK modulation at the wavelength center λ_0 = *1.31μm* with input power 3mW Gaussian CW modulated. All–optical OOK generation that is on-off state occurred within upper (out_1) and lower (out_2) MZI arm, with differences phase shift is equal to π.

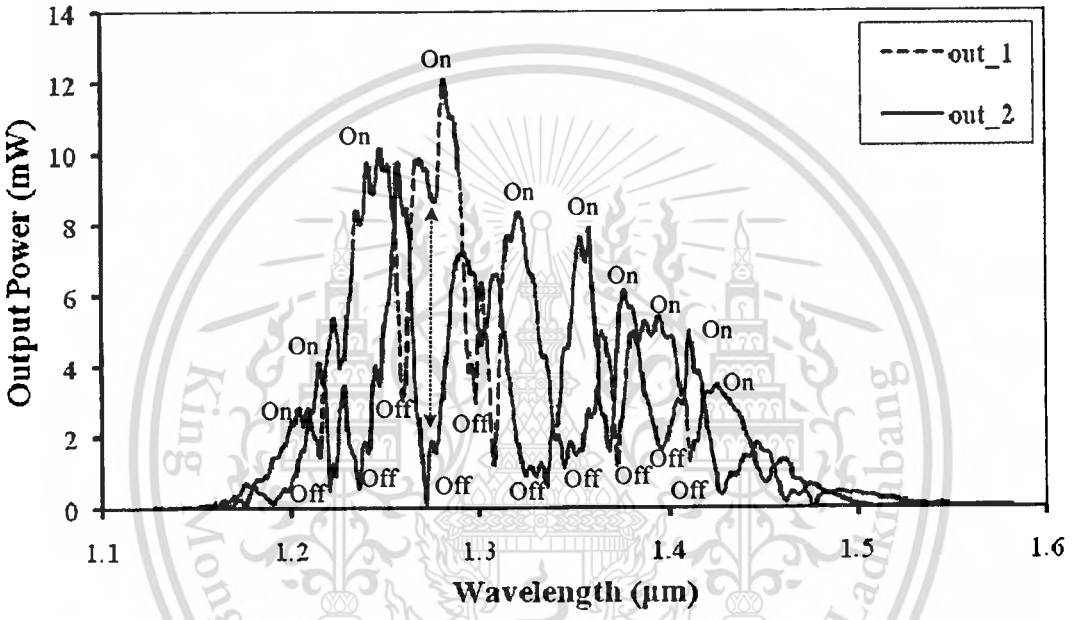

Figure 3.4 OOK result as generated at wavelength center λ_0 = *1.31μm* and input power 3mW.

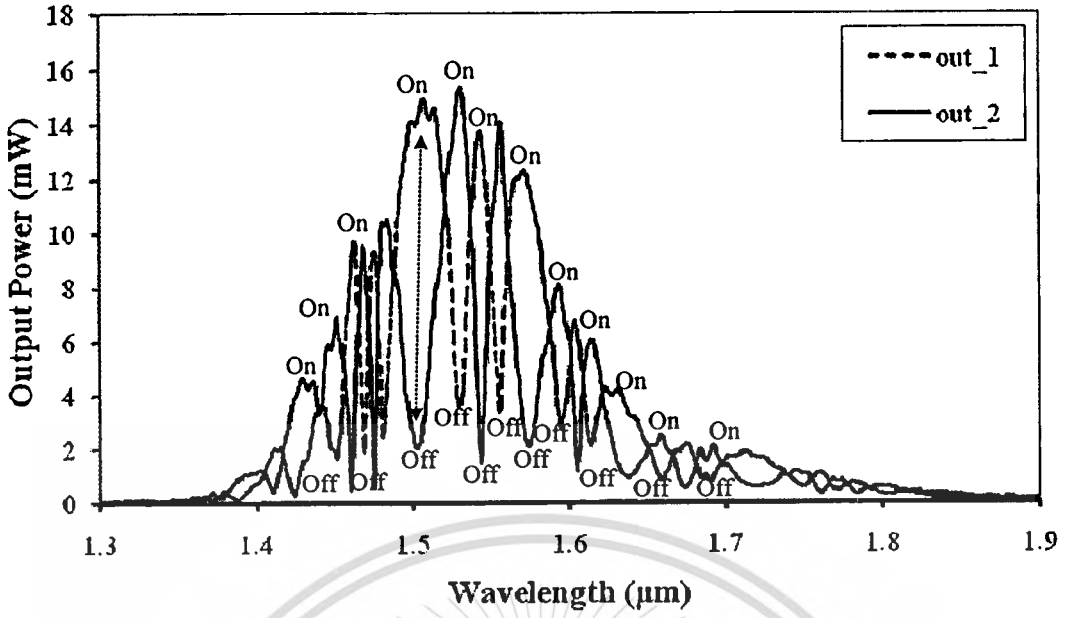

Figure 3.5 OOK result as generated at wavelength center $\lambda_0 = 1.55\mu m$ and input power 3mW.

In Figure 3.5, the numerical simulation OOK modulation at the wavelength center $\lambda_0 = 1.55\mu m$ with input power 3mW Gaussian CW modulated. All–optical OOK generation that is on-off state occurred within upper (out_1) and lower (out_2) MZI arm, with differences phase shift is equal to π. Output power of out_1 and out_2 numerical simulation OOK generated is faster where compare with generation at $\lambda_0 = 1.31\mu m$ and the delay time of on off state is 1.2fs, where the operation of the proposed circuit is transient in time as shown in Figure 3.6.

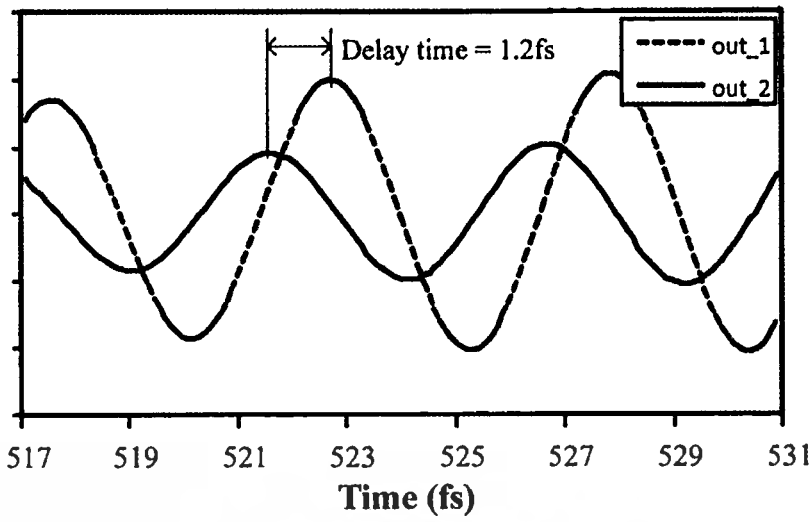

Figure 3.6 Delay time of OOK.

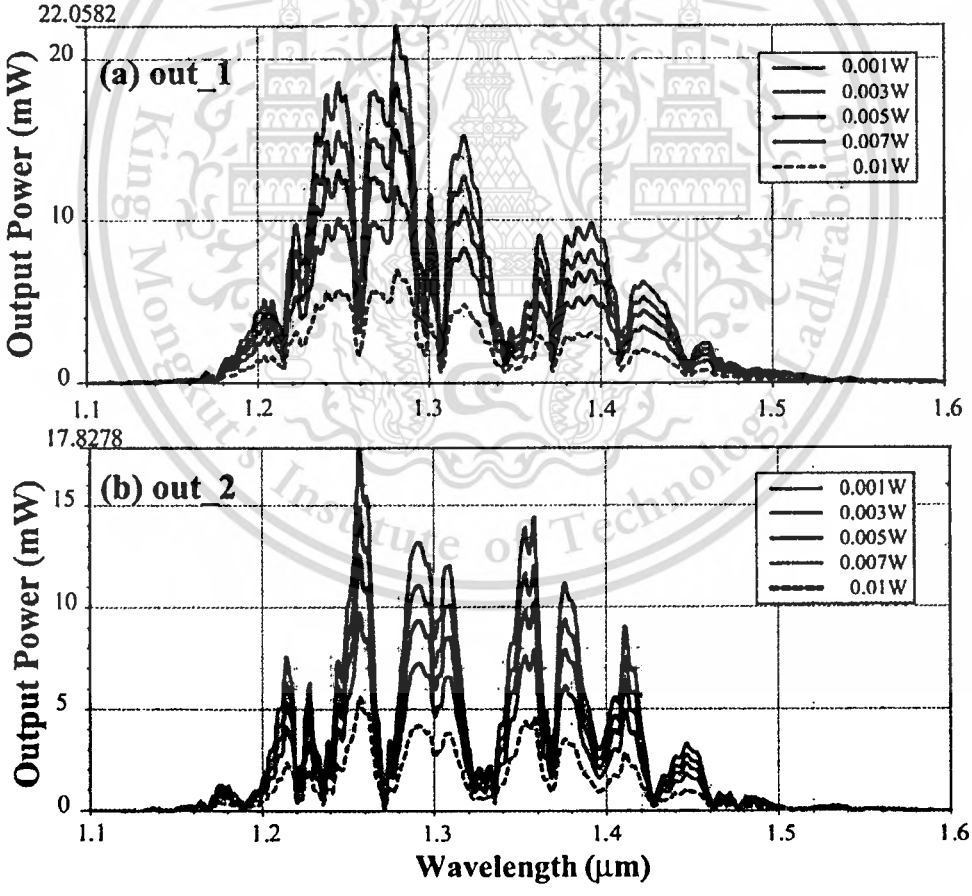

Figure 3.7 Simulation results for varies input power at the center wavelength 1.31μm.

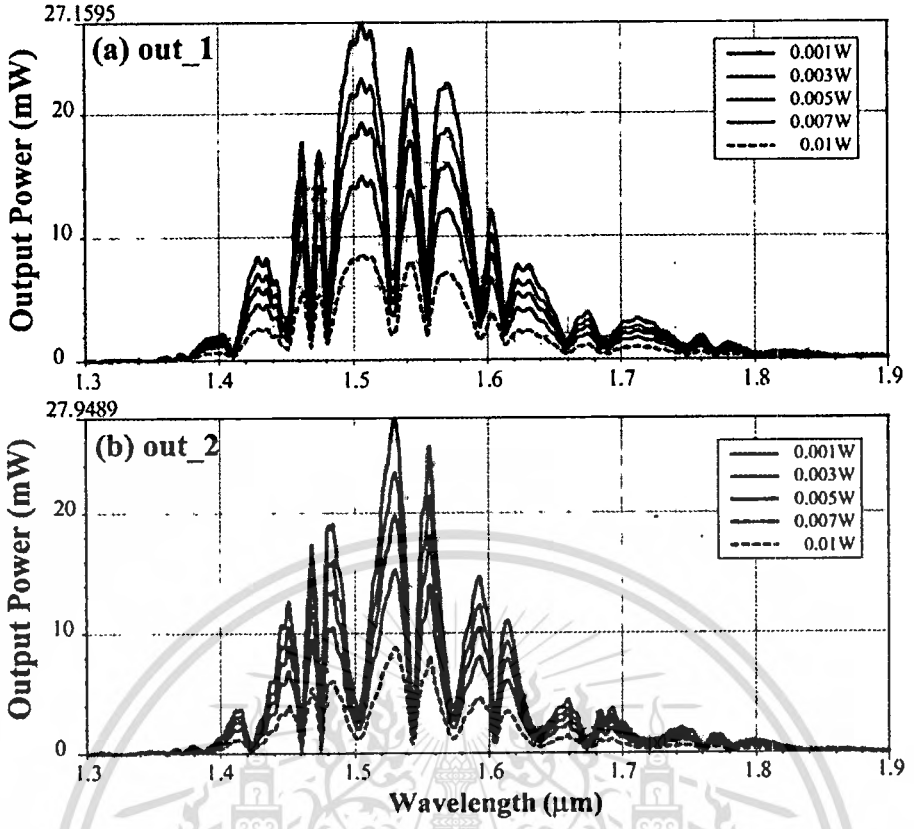

Figure 3.8 Simulation results for varies input power at the center wavelength 1.55μm.

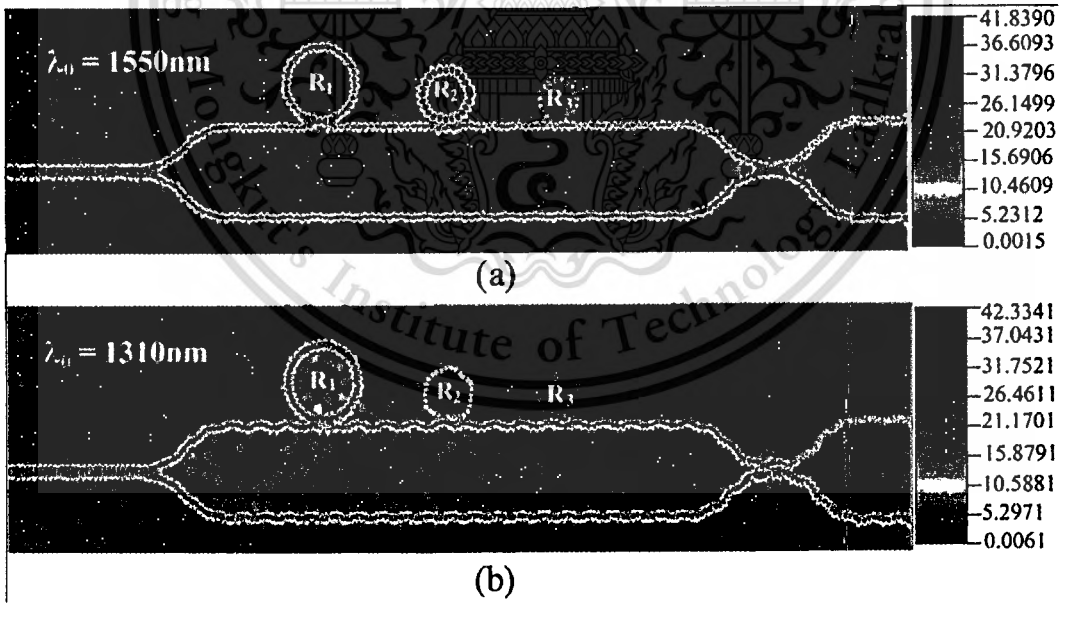

Figure 3.9 FDTD results of resonances (a) 1550nm and (b) 1310nm. I found that the resonance at R_2 for 1550nm and R_1 for 1310nm.

Table 3.1 Conclusion the output power for wavelength 1.31μm and 1.55μm

Center wavelength (μm)	Input Power (W)	Output Power (W)	
		Out_1	Out_2
1.31	0.001	6.6376	5.6376
	0.003	12.01	9.7647
	0.005	15.51	12.6062
	0.007	18.48	14.9158
	0.010	22.058	17.8278
1.55	0.001	8.5885	8.8382
	0.003	14.8759	15.3082
	0.005	19.8792	19.7628
	0.007	22.7232	23.3837
	0.010	27.1595	27.9489

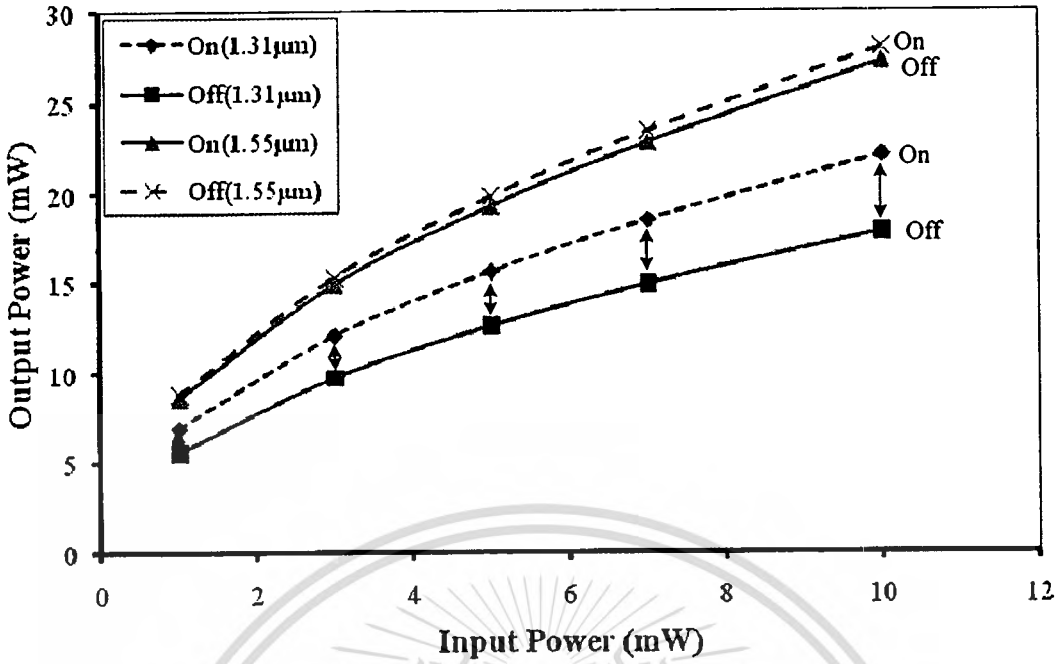

Figure 3.10 Compare OOK generate at wavelength center, $\lambda_0 = 1.55\mu m$ and $\lambda_0 = 1.31\mu m$, respectively.

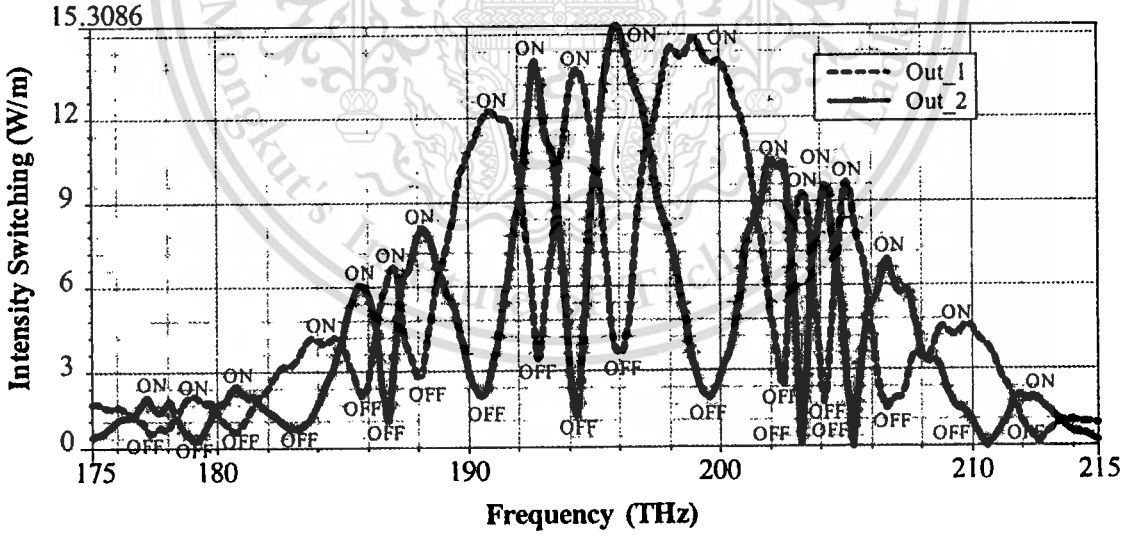

Figure 3.11 OOK result as generated in frequency domain and input power 3mW.

When increase the input from 1 – 10 mW I found that the output power is increased exactly. The phenomena are shown in figure 3.7 and 3.8 know as amplitude–shift keying (ASK)

is generated at wavelength center $\lambda_0 = 1.55\mu m$ and $\lambda_0 = 1.31\mu m$, respectively, the output power values are conclude in table 3.1. The resonances enhance are occurred at the second MRR (R_2) and first MRR (R_1) coupled to a MZI arm for input wavelength center $\lambda_0 = 1.55\mu m$ and $\lambda_0 = 1.31\mu m$, respectively, as shown in figure 3.9.

In Figure 3.10 shown OOK generated at wavelength center, $\lambda_0 = 1.55\mu m$ and $\lambda_0 = 1.31\mu m$, respectively and I found that the OOK at wavelength 1.55μm is switching faster than 1.31μm, therefore, the switching OOK generated at wavelength center 1.55μm that high capacity packet on–off state appearance. The upper limit of the circuit in frequency domain (response) is 3.5THz, which is obtained and shown in Figure 3.11.

3.4 Discussion and Conclusion

In this chapter have demonstrated the OOK modulation format by using NRRs coupled into one arm of a MZI system could be performed. The solution of the nonlinear Schrödinger equation is $E_{Li} = E_{Ri} \exp\left(-\frac{\alpha}{2} L_i - \gamma_{NL_i} |E_{Ri}|^2 L_i\right)$, which describes the nonlinear properties in each nonlinear ring resonator by using the term $|E_{Ri}|^2$ that circulates in each NRR. It is used to enhance and amplify the output signals. When the input light pulse is input through a 3dB coupler of a MZI, the coupling power is partially circulated through R_1, where it is circulated and combined with the pump light within R_1. Finally, the output of rings R_2 and R_3 are obtained in the similar manner.

The feasibility of the device by comparison to already fabricated devices with the same radius NRR radii, where $R_1 = 1.5\mu m$, $R_2 = 1.0\mu m$ *and* $R_3 = 0.775\mu m$. This parameter details are given by reference [63]. Our proposed system is the extended system of a Mach–Zehnder interferometer combined with ring resonators. It was fabricated by Rabus [62, 63], where the system size was 700 × 2500 μm^2. It is larger than the system in this paper where the system size is 10 × 40μm^2. Moreover, our system is combined with the triple nonlinear ring resonators. Two different results at the center wavelength 1.31μm and 1.55μm are compared, where they are

dominated by the nonlinear refractive indices and two–photon absorption coefficients within the NRRs. We found that the OOK generated at 1.55μm is shown the fastest switching, where the delay time of OOK is 1.2fs. We have also presented the principles of MZI operation in PSBT–based systems, where the characterization of useful parameters required for the DPSK demodulation or PSBT encoding. DPSK and PSBT have been highlighted as the suitable modulation formats for optical transmissions. The DPSK modulation format presents the better performance for transmission than the conventional OOK, justifying its utilization. However, the DPSK requires the passive MZIs for interferometric demodulation. In application, the use of DWDM (Dense Wavelength Division Multiplexing) can be employed to obtain the multi–wavelength OOK, which may be available for high capacity packet switching.

CHAPTER 4

Novel Tunable Dynamic Tweezers using Dark–Bright Solitons Collision Control in an Optical Add/Drop Filter

In this chapter propose a novel system of the tunable dynamic optical tweezers using a generated dark soliton in the fiber optic loop. A dark soliton known as an optical tweezers is amplified and tuned within the ring resonator system. The required tunable tweezers with different width and power can be controlled. The analysis of dark–bright soliton conversion using a dark soliton pulse propagating within a microring resonator system is analyzed. The dynamic behaviors of soliton conversion in add/drop filter is also analyzed. The control dark soliton is input into the system via the add port of the add/drop filter, where the dynamic behavior of the dark–bright soliton conversion is seen. The required stable signal is obtained via a drop and throughput ports of the add/drop filter with some suitable parameters. In application, the dynamic optical tweezers can be configured by the dark–bright soliton conversion system. Therefore, the use of trapped light/atom can be covered by using the proposed system.

4.1 Introduction

Optical tweezers are a powerful tool for use in the three-dimensional rotation of and translation (location manipulation) of nano–structures such as micro–and nano–particles as well as living microorganisms [20]. The benefit offered by optical tweezers is the ability to interact with nano–scaled objects in a non-invasive manner, i.e. there is no physical contact with the sample, thus preserving many important characteristics of the sample, such as the manipulation of a cell with no harm to the cell. Optical tweezers are now widely used and they are particularly powerful in the field of microbiology [21] – [24] to study cell–cell interactions, manipulate organelles without breaking the cell membrane and to measure adhesion forces between cells. To make the familiarity for such a new combination area, firstly, the theoretical description of optical

soliton is reviewed, where more details can also be found in many references, especially, one of them which is well analyzed by Agrawal [25]. Secondly, a new concept of developing an optical tweezers source using a dark soliton pulse is demonstrated. The developed tweezers has many potential applications in electron, ion, atom and molecule probing and manipulation as well as DNA probing and transportation [26, 27]. Furthermore, the soliton pulse generator is a simple and compact design, making it more commercially viable. In principle, the change in potential value, i.e. gradient of potential of the dark soliton pulse can produce force that can be used to confine/trap atoms/molecule. Furthermore, the change in potential well is still stable in some conditions, which mean that the dynamic optical tweezers is plausible. Finally, we present the very interesting work of the use of a dark soliton pulse beam that has potential applications in the probing and transport of atoms or molecules as an optical tweezers, which is important to ensure that the transported atom/molecule is not lost in the link media. The theoretical background of the trapped atom/molecule is also analyzed and described in details. The system design of the tweezers amplification, tunable and storage is also analyzed for the use of atom/molecule probing and assembly.

In this chapter, the dark soliton pulse was experimentally generated using a pumped fiber optic loop. The obtained dark soliton can be amplified and tuned by using the nonlinear ring resonator system analytically. The tunable tweezers (dark soliton) is controlled by using the dark–bright soliton conversion control. The dynamic behaviors of soliton conversion, i.e. tunable optical tweezers within an add/drop filter is analyzed. The multiplexed signals with different wavelengths into the system is also available via the add port, which means the use of atom/molecule transportation in the network is possible.

4.2 Theory and Principle

Optical solitons can naturally be divided into classes of dark and bright solitons. Specific, a dark soliton exhibits an interesting and remarkable behavior, when it is transmitted into an optical transmission system. It has the advantage of signal security, when the ambiguity of signal detection becomes a problem of the un–required users. Recently, Sarapat et al [41] have shown

that the conversion of a dark soliton into a bright soliton can be realized using an add/drop filter. Here the secured signals in the transmission are retrieved using a suitable an add/drop filter that is connected to the transmission line. The other promising application of a dark soliton signal is confirmed by using the large guard band of two different frequencies which can be achieved by using a dark soliton generation scheme and trapping a dark soliton pulse within a nano ring resonator [42, 43]. Furthermore, the dark soliton pulse shows a more stable behavior than the bright solitons with respect to the perturbations such as amplifier noise, fiber losses, and intra-pulse stimulated Raman scattering [25]. It is found that the dark soliton pulses propagation in a lossy fiber, spreads in time at approximately half the rate of bright solitons. Heidari et al [44] have shown that the multichannel wavelength conversion using three different types of dispersion profiles along the optical fibers. The dark solitons trapped in add/drop system is realized, therefore, optical tweezers appearance relation between scattering and gradient force of light propagation. Yuan et al [45] have shown an abruptly tapered twin–core fiber optical tweezers, by using two–beam combination technique and found that a strong enough gradient forces well tapered twin–core fiber optical tweezers. Optical tweezers were also characterized in terms of the optical potential well by measuring the displacement of trapped particles experiencing a viscous drag at a fluid flow below the critical velocity [46]. We are looking for a stationary dark soliton pulse, which is introduced into the multistage microring resonators as shown in Figure 4.1. The input optical field (E_{in}) of the dark soliton pulse input is given by [25, 47]

$$E_{in}(t) = A\tanh\left[\frac{T}{T_0}\right]\exp\left[\left(\frac{z}{2L_D}\right) - i\omega_0 t\right] \tag{4.1}$$

where A and z are the optical field amplitude and propagation distance, respectively. T is a soliton pulse propagation time in a frame moving at the group velocity, $T = t - \beta_1 * z$, where β_1 and β_2 are the coefficients of the linear and second-order terms of Taylor expansion of the propagation constant. $L_D = T_0^2/|\beta_2|$ is the dispersion length of the soliton pulse. T_0 in equation is a soliton pulse propagation time at initial input (or soliton pulse width), where t is the soliton phase shift time,

and the frequency shift of the soliton is ω_0. This solution describes a pulse that keeps its temporal width invariance as it propagates, and thus is called a temporal soliton. When a soliton of peak intensity $\left(\left|\beta_2/\Gamma T_0^2\right|\right)$ is given, then T_0 is known. For the soliton pulse in the microring device, a balance should be achieved between the dispersion length (L_D) and the nonlinear length ($L_{NL}=1/\Gamma\phi_{NL}$), where $\Gamma=n_2*k_0$, is the length scale over which dispersive or nonlinear effects makes the beam become wider or narrower. For a soliton pulse, there is a balance between dispersion and nonlinear lengths. Hence $L_D = L_{NL}$.

When light propagates within the nonlinear medium, the refractive index (n) of light within the medium is given by

$$n = n_0 + n_2 I = n_0 + \frac{n_2}{A_{eff}} P, \tag{4.2}$$

where n_0 and n_2 are the linear and nonlinear refractive indexes, respectively. I and P are the optical intensity and optical power, respectively. The effective mode core area of the device is given by A_{eff}. For the microring resonator (MRR) and nanoring resonator (NRR), the effective mode core areas range from 0.50 to 0.10 μm^2 [48, 49]. When a soliton pulse is input and propagated within a MRR, as shown in Figure 5.1, which consists of a series MRRs. The resonant output is formed, thus, the normalized output of the light field is the ratio between the output and input fields [$E_{out}(t)$ and $E_{in}(t)$] in each roundtrip, which is given by [41]

$$\left|\frac{E_{out}(t)}{E_{in}(t)}\right|^2 = (1-\gamma)\left[1 - \frac{\left(1-(1-\gamma)x^2\right)\kappa}{\left(1-x\sqrt{1-\gamma}\sqrt{1-\kappa}\right)+4x\sqrt{1-\gamma}\sqrt{1-\kappa}\sin^2\left(\frac{\phi}{2}\right)}\right] \tag{4.3}$$

The close form of Eq. (4.3) indicates that a ring resonator in this particular case is very similar to a Fabry–Perot cavity, which has an input and output mirror with a field reflectivity, $(1-\kappa)$, and a fully reflecting mirror. κ is the coupling coefficient, and $x = \exp(-\alpha L/2)$ represents a roundtrip loss coefficient, $\phi_0 = kLn_0$ and $\phi_{NL} = kLn_2|E_{in}|^2$ are the linear and nonlinear phase shifts,

$k = 2\pi/\lambda$ is the wave propagation number in a vacuum, where L and α are waveguide length and linear absorption coefficient, respectively. In this work, the iterative method is introduced to obtain the results as shown in Eq. (4.3), and similarly, when the output field is connected and input into the other ring resonators.

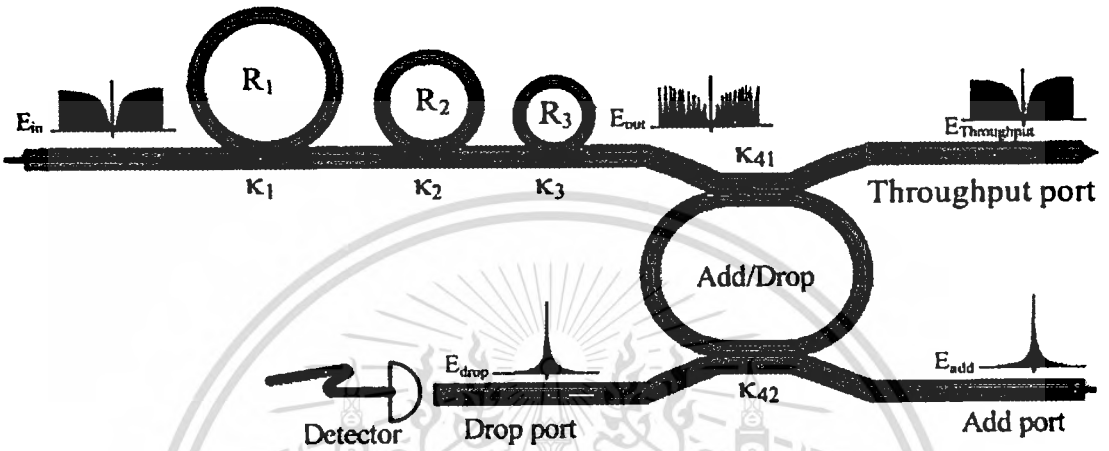

Figure 4.1 Schematic of a dark–bright soliton conversion system, where R_s is the ring radii, κ_s is the coupling coefficient, and κ_{41} and κ_{42} are the add/drop coupling coefficients.

To retrieve the signals from the chaotic noise, we propose to use the add/drop device with the appropriate parameters. This is given in the following details. The optical circuits of ring resonator add/drop filters for the throughput and drop port can be given by Eqs. (4.4) and (4.5), respectively [41].

$$\left|\frac{E_t}{E_{in}}\right|^2 = \frac{(1-\kappa_1)-2\sqrt{1-\kappa_1}\sqrt{1-\kappa_2}e^{-\frac{\alpha}{2}L}\cos(k_n L)+(1-\kappa_2)e^{-\alpha L}}{1+(1-\kappa_1)(1-\kappa_2)e^{-\alpha L}-2\sqrt{1-\kappa_1}\sqrt{1-\kappa_2}e^{-\frac{\alpha}{2}L}\cos(k_n L)} \tag{4.4}$$

and

$$\left|\frac{E_d}{E_{in}}\right|^2 = \frac{\kappa_1\kappa_2 e^{-\frac{\alpha}{2}L}}{1+(1-\kappa_1)(1-\kappa_2)e^{-\alpha L}-2\sqrt{1-\kappa_1}\sqrt{1-\kappa_2}e^{-\frac{\alpha}{2}L}\cos(k_n L)} \tag{4.5}$$

where E_t and E_d represent the optical fields of the throughput and drop ports, respectively. $\beta = kn_{eff}$ is the propagation constant, n_{eff} is the effective refractive index of the waveguide, and the circumference of the ring is $L = 2\pi R$ with R as the radius of the ring. In the following, new parameter is used for simplification with $\phi = \beta L$ as the phase constant. The chaotic noise cancellation can be managed by using the specific parameters of the add/drop device, and the required signals can be retrieved by the specific users. κ_1 and κ_2 are the coupling coefficient of the add/drop filters, $k_n = 2\pi/\lambda$ is the wave propagation number for in a vacuum, and where the waveguide (ring resonator) loss is $\alpha = 0.5\ dBmm^{-1}$. The fractional coupler intensity loss is $\gamma = 0.1$. In the case of the add/drop device, the nonlinear refractive index is neglected.

4.3 Optical Tweezers Generation

An Optical Spectrum Analyzer (OSA) with a resolution of *0.07 nm* is used to analyze the output of the proposed setup. The operation of the experimental setup is also follows; the BP generates a 1500 nm signal at 1.96 dBm, where it enters Port 1 of the first OC. The signal then travels onward to the DCF, where the non-linear interactions will provide the first Stokes wavelength. The BP and Stokes then travels onwards to the second OC where it is reflected back to the DCF and again to Port 2 of the first OC, where it will now exit via Port 3 which is connected to the OSA.

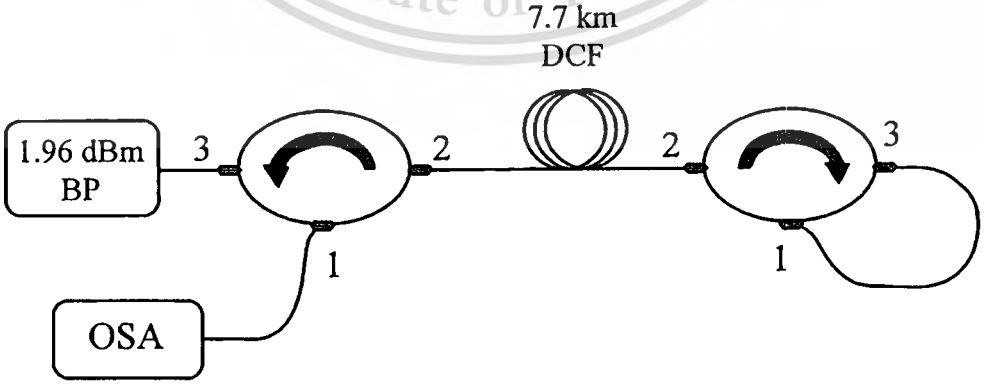

Figure 4.2 Shows an experimental setup for optical tweezers generation.

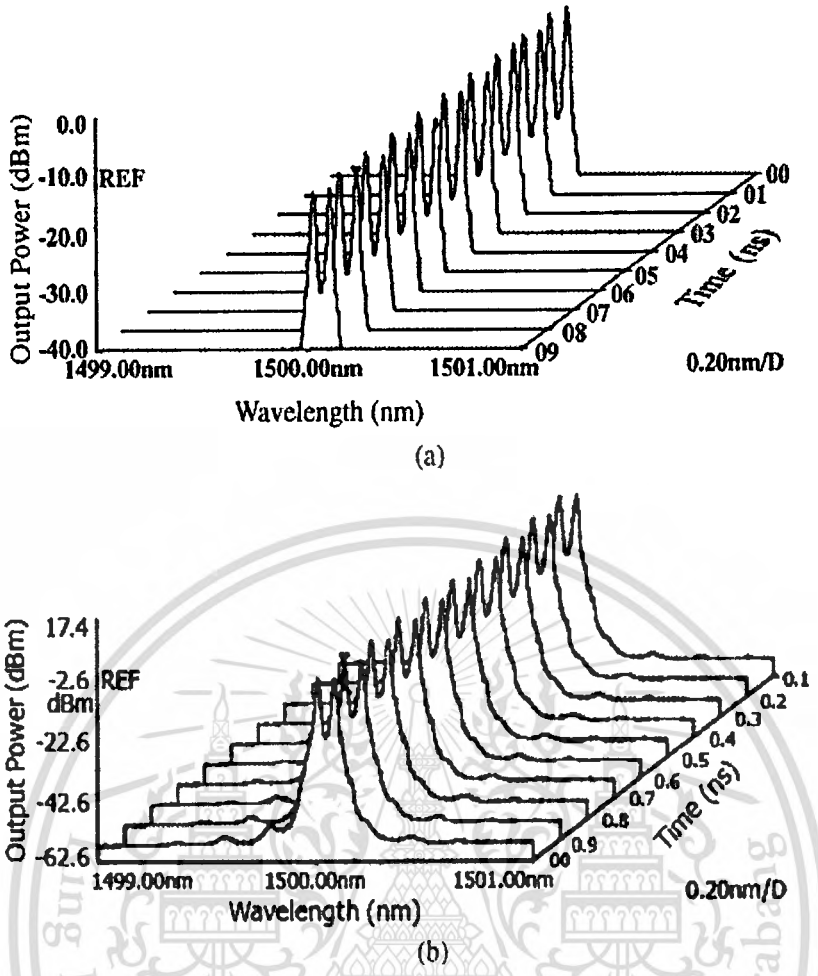

Figure 4.3 Show dark soliton propagation over time, which is similar to a potential well.

The experimental setup is shown in Figure 4.2. The dark soliton generator consists of a fiber laser based on a non-linear gain medium that is placed in a linear cavity. The nonlinear gain medium is a 7.7 km Dispersion Compensating Fiber (DCF) which is pumped by a 1500 nm Brillouin Pump (BP) at 1.96 dBm. An Optical Circulator (OC) is used at one end of the setup to act as a fiber based mirror, with Port 3 connected to Port 1 while Port 2 is connected to the rest of the experimental setup. Another OC is also used in the experimental setup to guide the incoming and outgoing signals. From Figure 4.3, the soliton propagation over time can be obtained. As can be seen in the figure, the soliton pulse maintains its shape through the time of testing with no observable fluctuation in the power or wavelength. This is critical as any slight fluctuation will cause the beam to lose its hold over the transported atom or molecule, effectively dropping it.

4.4 Dark–Bright Soliton Conversion

Experimentally, the generated dark soliton pulse, for instance, with 50ns pulse width, and a maximum power of $0.65W$ is input into the dark–bright soliton conversion system, as shown in Figure 4.1. The suitable ring parameters are used, such as ring radii where $R_1=10.0\mu m$, $R_2=7.0\mu m$, and $R_3=5.0\mu m$. In order to make the system associate with the practical device [48, 49], whereas the selected parameters of the system are fixed to $\lambda_0=1.50\mu m$, $n_0=3.34$ (InGaAsP/InP). The effective core areas are $A_{eff}=0.50,\ 0.25$, and $0.10\ \mu m^2$ for a MRR and NRR, respectively. The waveguide and coupling loses are $\alpha=0.5dBmm^{-1}$ and $\gamma=0.1$, respectively, and the coupling coefficients κ_s of the MRR are ranged from 0.05 to 0.90. However, more parameters are used as shown in Figure 4.1. The nonlinear refractive index is $n_2=2.2\times10^{-13}$ m^2/W. In this case, the waveguide loss used is $0.5\ dBmm^{-1}$. The input dark soliton pulse is chopped (sliced) into the smaller signals, where the filtering signals within the rings R_2 and R_3 are seen. I find that the output signals from R_3 are smaller than from R_1, which is more difficult to detect when it is used in the link. In fact, the multistage ring system is proposed due to the different core effective areas of the rings in the system, where the effective areas can be transferred from 0.50 to $0.10\mu m^2$ with some losses. The soliton signals in R_3 is entered in the add/drop filter, where the dark–bright soliton conversion can be performed by using Eqs. (4.4) and (4.5). Results obtained when a dark soliton pulse is input into a MRR and NRR system as shown in Figure 4.4. The add/drop filter is formed by using two couplers and a ring with radius (R_d) of $10\mu m$, the coupling constants (κ_{41} and κ_{42}) are the same values (0.50). When the add/drop filter is connected to the third ring (R_3), the dark–bright soliton conversion can be seen. The bright and dark solitons are detected by the through (throughput) and drop ports as shown in Figure 4.4(a) – (e), respectively.

4.5 Tunable Dynamic Tweezers

In application, the dynamic optical tweezers is occurred, when we added bright soliton input at the add port with shown in Figure 4.1, the parameters of system are set the same as the

previous section. The bright soliton was generated at the central wavelength $\lambda_0 = 1.5\mu m$, when the bright soliton propagating into the add/drop system, the occurrence of dark–bright soliton collision in add/drop system is shown in Figure 4.5(a) – (d) and Figure 4.6(a) – (d).

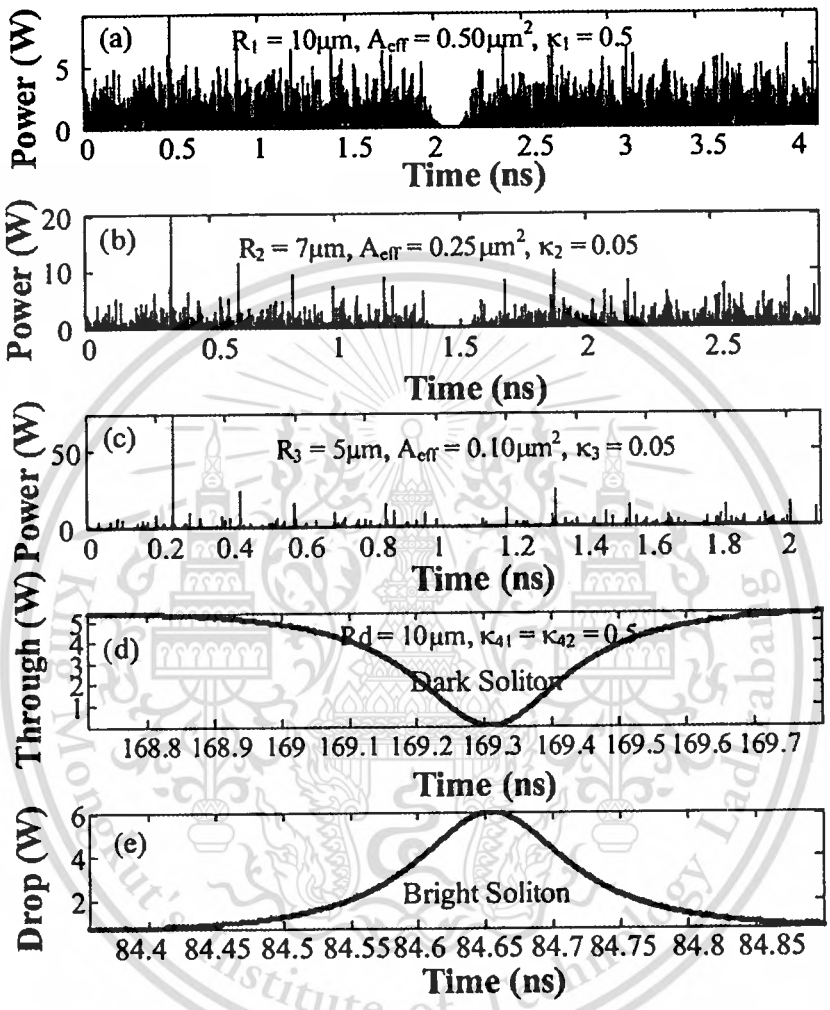

Figure 4.4 Results of the soliton signals within the ring resonator system, where (a) R_1, (b) R_2, (c) R_3, and (d) – (e) dark–bright solitons conversion at the add/drop filter. The input dark soliton power is 2W.

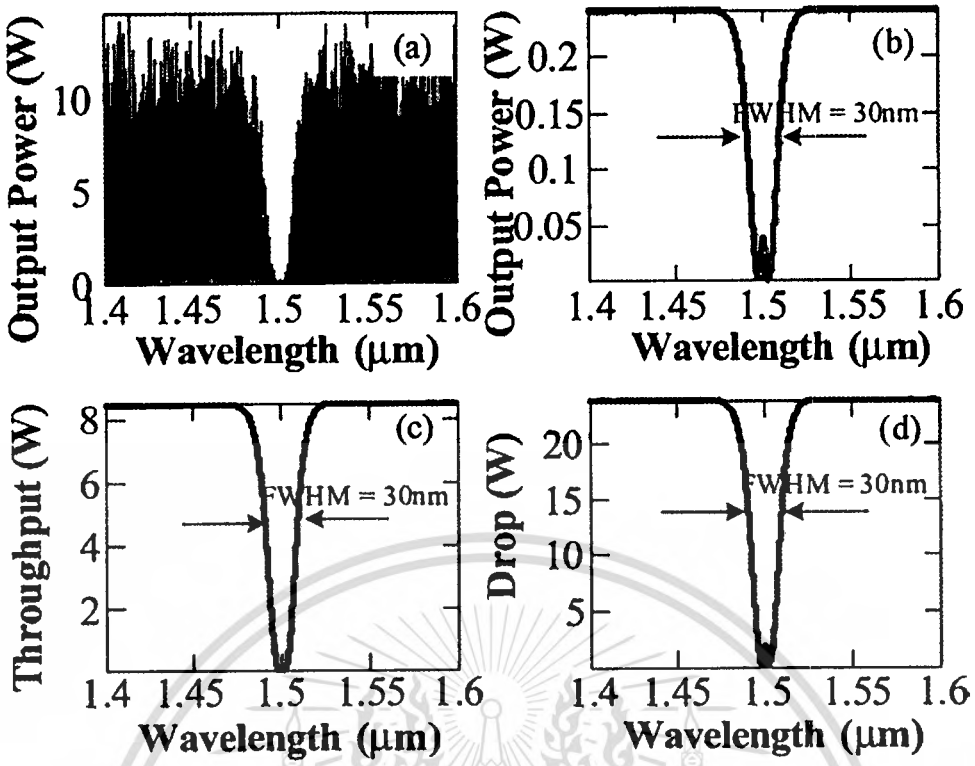

Figure 4.5 The dynamic optical tweezers output within the add/drop filter, when the bright soliton input with the central wavelength $\lambda_0 = 1.5\mu m$, where (a) add/drop signal, (b) dark–bright soliton collision, (c) optical tweezers at throughput port, and (d) optical tweezers at drop port.

The optical tweezers probe can be trapped/confined atom/light by using the appropriate probe, which can be tuned to meet the specific requirement. The stability of the dual Brillouin is shown in Figure 4.3. The dark soliton valley dept, i.e. potential well, is changed when it was modulated by the trapping energy (dark–bright solitons interaction) as shown in Figure 4.6(a) – (d). The trapping of photon within the dark well is occurred and seen, the recovery photon can be obtained by using the dark–bright soliton conversion, which is well analyzed by Sarapat et al. [41], where the trapped photon or molecule can be released an seen separately from the dark soliton pulse, in practice, in this case the bright soliton is become alive and seen.

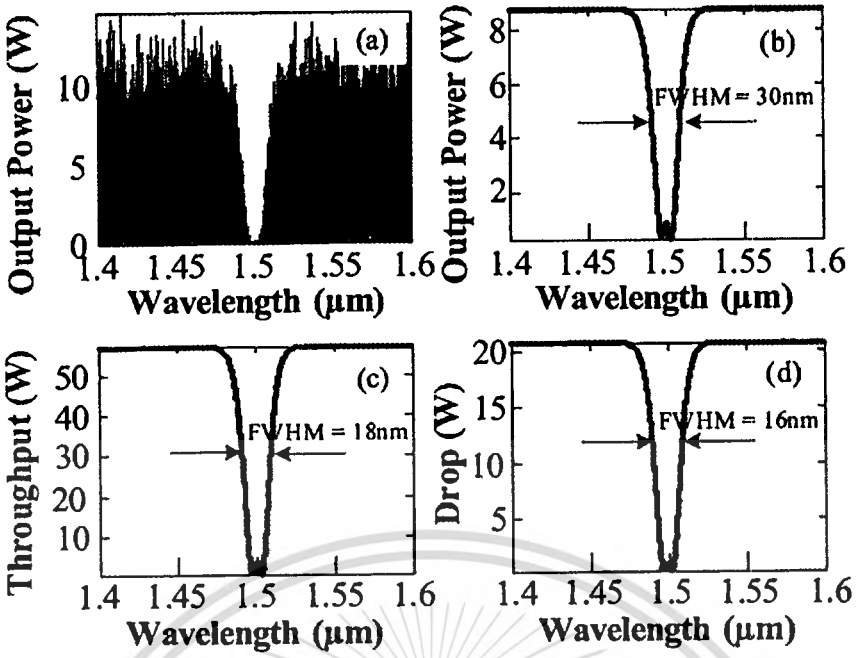

Figure 4.6 The tuned dynamic optical tweezers output within the add/drop filter, when the bright soliton input with the central wavelength $\lambda_0 = 1.5\mu m$, where (a) the add/drop signal, (b) dark–bright soliton collision, (c) optical tweezers at throughput port, and (d) optical tweezers at drop port.

4.6 Conclusion

In this chapter, I have demonstrated that after the dark soliton pulse was generated by using the pumped laser system. I have shown that the propagating dark soliton within the MRR and NRR system can be converted to be a bright soliton by using the ring resonator system, incorporating the add/drop multiplexer, moreover, the amplification and tenability of the dark soliton pulse can be obtained. By using the reasonable dark–bright soliton input power, the tunable optical tweezers can be controlled, which can be used as the dynamic optical tweezers probe. In application, such a behavior can be used to confine the suitable size of light pulse or molecule, which can be employed in the same way of the optical tweezers. But in this case the terms dynamic probing is come to be a realistic function. Moreover, the transportation of the trapped pulse or molecule is plausible.

CHAPTER 5

Low Power Ultrafast Switching Generation Based on NMRs Coupled into a MZI Arm

In this chapter, I propose a new method of ultrafast switching generation using low power coupled into NMRs in a MZI arm, where in this operation the input power of 3mW is required. Mathematical derivation of the system is analyzed, and the simulation results are obtained by using FDTD method. We have found that the ultrafast packet switching delay time can be controlled by the coupled NMRs, where in this work the shortest packet switching delay time of 8 fs is obtained.

5.1 Introduction

All–optical switches have been extensively investigated for the implementation of the ultrafast optical networks, especially, when the high capacity data transmission is required, in which the use ultrafast switching based on photonic crystal nanocavity [28, 29], spin–polarized surface–normal optical switches [30] and digital optical circuits and their use in packet switching [31] have been reported. However, the switching operation improvements are still required, here, the improvement of orthogonal ASK/DPSK optical label switching performance by DC–balanced line encoding [32] and low threshold and tunable all–optical switch using two–photon absorption in array of nonlinear ring resonators coupled to MZI [17] are included. More research works in various schemes are also included, for instance, the use of all–optical ultrafast switching can be controlled by using a high–nonlinear micro ring coupled MZI through a pumped nonlinear coupler [18], an EDF–ring coupled M–Z interferometer [33], asymmetric Fano resonance and bistability for high extinction ratio, large modulation depth, and low power switching [34], THz electro–absorption effect enabling femtosecond all–optical switching in semiconductor quantum dots [35], nonosecond switching and

wavelength tuning of external–cavity laser diode using a reflective electroabsorption modulator [36], detailed design and characterization of all–optical switches based on InAs/GaAs quantum dots in a vertical cavity [37], threshold voltage and mobility extraction by ultrafast switching measurement on NBTI [38]. Till date, the ultrafast switching improvement, especially, ultrafast packet switching is still required. Recently, the ultrafast packet switching generation using a nonlinear microring resonator for secure packet switching application has been proposed, where more recently, the use of OOK ultrafast switching generation based on MZI incorporating a pumped nonlinear ring resonators system [39] has also been reported, in which the reports of switching speeds for such devices are on the order of *ps*. Therefore, in this paper, we propose a scheme for generating ultrafast switching with low power input based on nonlinear microring resonators (NMRs) coupled into a MZI arm. In order to increase the bit–rate of on-chip optical links by using FDTD method [40], in which the nonlinear behavior of light within the (NMRs) can be used to analyze for low power ultrafast switching modulation. The NMRs are coupled into a MZI arm structure and the details given. Moreover, the NMRs are used for a phase shifted devices by coupling into one arm of a MZI [39]. In this structure, one arm presents an optical delay line equal to the bit duration time. The MZI characteristics for the two applications are slightly different, which will be seen in the next sections. The novelty of this work is that the nonlinear light pulses generated by using the multi NMRs in one arm of a Mach–Zehnder interferometer can be used to enhance (amplify) the packet switching signals, where the increasing in switching sped and delay switching time can be obtained by using the coupled nonlinear ring resonators, where in this work the nonlinear coefficient refractive index of nonlinear ring resonator (GaInAsP/InP) is $n_2 = 2.2\times10^{-13}\ m^2/W$.

5.2 Operating Principle

I propose the use of the system as shown in Figure 5.1(a) for low power ultrafast switching generation model, where the increasing in switching time and packet switching capacity can be generated and obtained. Three nonlinear microring resonators (NMRs) are coupled into one arm of

Mach–Zehnder interferometer, in which NMRs have the same field–dependent absorption and refractive index coefficients.

When the input field, E_{in}, is entered and split into two MZI arms with power ratio 50:50, the mathematical expression can be given by

$$E_{11} = \sqrt{1-k}E_{in}, \tag{5.1}$$

$$E_{21} = \sqrt{1-k}E_{in}, \tag{5.2}$$

Here $k = 0.5$ is the power coupling ratio.

According to the linear coupling theory, the following relations can be connected into input–output fields for each NMR as shown in Figure 5.1(b), which can be expressed by [39]

$$E_{Ri,1} = \sqrt{1-g_i}E_{Ri,2} + j\sqrt{g_i}E_{11}, \tag{5.3}$$

$$E_{T_i} = \sqrt{1-g_i}E_{11} + j\sqrt{g_i}E_{Ri,2}, \tag{5.4}$$

$$E_{Ri,2} = E_{Ri,1}e^{-\frac{\alpha}{2}L_i - i\phi_i}, \tag{5.5}$$

Here g_i is the coupling gap in each nonlinear microring coupled to bus waveguide by $i = 1,2,3$, $L_i = 2\pi R_i$, R_i is the radius of NMR, E_{T_i} is the output field of each NMR, and $E_{Ri,1}, E_{Ri,2}$ are the circulated field of each NMR as shown in Figure 5.1(b). α is the loss coefficient of the nonlinear microring, ϕ_i is the round–trip phase in the NMR, which is given by

$$\phi_i = \tan^{-1}\left[\frac{-g_i \sin\left(\frac{\omega_0}{c}n_2 L_i \left|E_{Ri,2}\right|^2\right)}{2\sqrt{1-g_i} - (2-g_i)\cos\left(\frac{\omega_0}{c}n_2 L_i \left|E_{Ri,2}\right|^2\right)}\right]. \tag{5.6}$$

Here ω_0, c and n_2 are the incident light frequency, speed of light in free space and the nonlinear index of refraction coefficient, respectively. The following relation describes the nonlinear phenomenon in the NRRs as

Substitute (5.5) into (5.3), we yield,

$$E_{Ri,1} = \frac{j\sqrt{g_i}E_{11}}{1-\sqrt{1-g_i}e^{-\frac{\alpha}{2}L_i - i\phi_i}}, \tag{5.7}$$

Similarly, from (5.4) we yield,

$$E_{T_i} = \frac{\sqrt{1-g_i} - e^{-\frac{\alpha}{2}L_i - i\phi_i}}{1-\sqrt{1-g_i}e^{-\frac{\alpha}{2}L_i - i\phi_i}} E_{11}, \tag{5.8}$$

When light propagates through the second gap coupler of MZI, with the coupler gap coefficient is K. The amplitude–shift keying (ASK) and phase–shift keying (PSK) are controlled by the optical pump in each NMR of upper and lower MZI arms, respectively, which is given by

$$\begin{pmatrix} E_{out\_1} \\ E_{out\_2} \end{pmatrix} = \begin{pmatrix} \sqrt{1-\kappa} & j\sqrt{\kappa} \\ j\sqrt{\kappa} & \sqrt{1-\kappa} \end{pmatrix} \begin{pmatrix} E_{12} \\ E_{22} \end{pmatrix}. \tag{5.9}$$

Here, for phase–shift keying (PSK), the difference phase shift is equal to π [39].

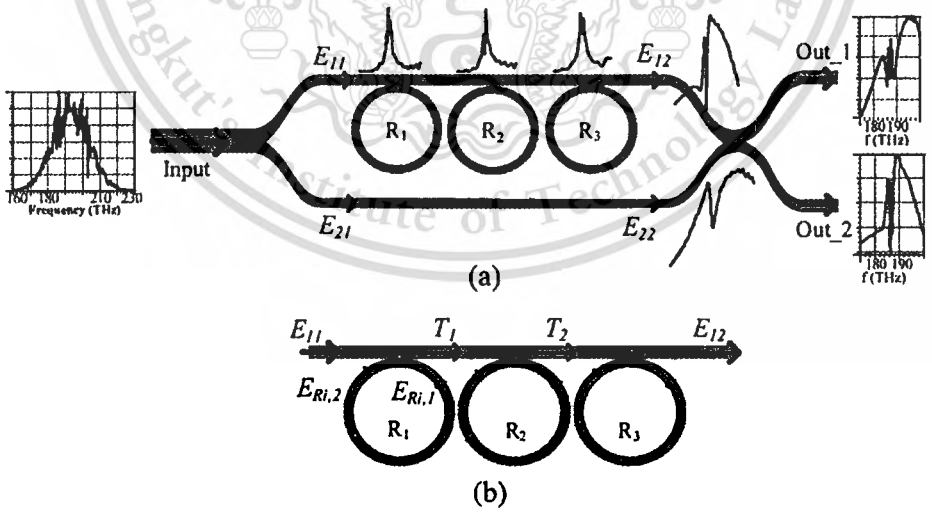

Figure 5.1 Schematic diagram of (a) three microring resonators (TR) coupled to one Mach–Zehnder interferometer arm for APSK generated in InGaAsP/InP waveguide size 15 × 50μm^2, with a coupling gap of 6nm. (b) TR coupled to a single–bus waveguide.

5.3 Results and Discussion

In operation, the system is as shown in Figure 5.1(a), the MZI width and depth is 0.3μm and 0.5μm, respectively. The microring radii are 1.5μm, with $n_0=3.34$ (GaInAsP/InP waveguide). The CW Gaussian modulated pulse with $3mW$ peak power at center wavelength $\lambda_0=1.55\mu m$, $40\,fs$ time offset, 15 fs half width is input into the system. In simulation, the numerical results are obtained by using the commercially available simulation software called the OptiFDTD simulation package [40]. Here, three amplitude level signals are generated by using three symmetric microring resonators, which they are arranged in series in a Mach–Zehnder configuration as seen in Figure 5.1(a), in which light is split into two separated paths by a 3–dB coupler (50:50). When light is in the resonant condition with the NMRs, it is coupled into the out_1 ports, in which the constructively interfered at the output port is seen. If one NMR is shifted off-resonance, it is only half of the light being transferred to the out_2 port as illustrated in Figure 5.1(a).

Figure 5.2 shows the comparison results of the switching windows generated by using a single nonlinear microring resonator (SR), double nonlinear microring resonator (DR), and triple nonlinear microring resonator (TR) coupled to one arm of MZI as shown in Figure 5.2(a) – (c). We found that the enhanced the switching window (grey band) is increased from ~6.6 fs to 10 fs, which can be used to increase the packet switching(bit rate). The phase shift keying (PSK) enhancement is equal to π [39], the switching threshold I_{th} decreases from 20.06 fs to 19.89 fs. In Figure 5.3, when the triple–NMRs are coupled into the system, the faster switching time than the single–NMR is seen, where the full width at half maximum (FWHM) are decreased to 2.9822THz, 2.2873THz and 2.0389THz as shown in Figure 5.3(a) – (c), respectively. In Figure 5.4, we found that the delay time of single–NMR is equal to 16.0984 fs, in which when more NMRs are coupled into the upper MZI arm, the delay time is reduced to 15.0134 fs and 13.6804 fs respectively, as shown in Figure 5.4(b) and Figure 5.4(c).

For further investigation, a scheme of all–optical switching using NMRs is as shown in Figure 5.5, where there are seven NMRs coupled to one MZI arm, which can be used to form the hybrid packet ultrafast switching generation with all NMRs with the same ring material (GaInAsP/InP waveguide), the ring radii are 1.5μm. In Figure 5.6, result of the ultrafast switching of seven–NMRs coupled into MZI arm is seen, which we found that the enhanced switching window is equal to ~13.3 fs, the switching threshold I_{th} is 15.01 fs. Result of the ultrafast packet switching of seven–NMRs coupled into MZI arm is shown in Figure 5.7, which we found that the delay time equal to 8 fs is seen. Finally, the dynamic pulse train of seven–NMRs is as shown in Figure 5.8.

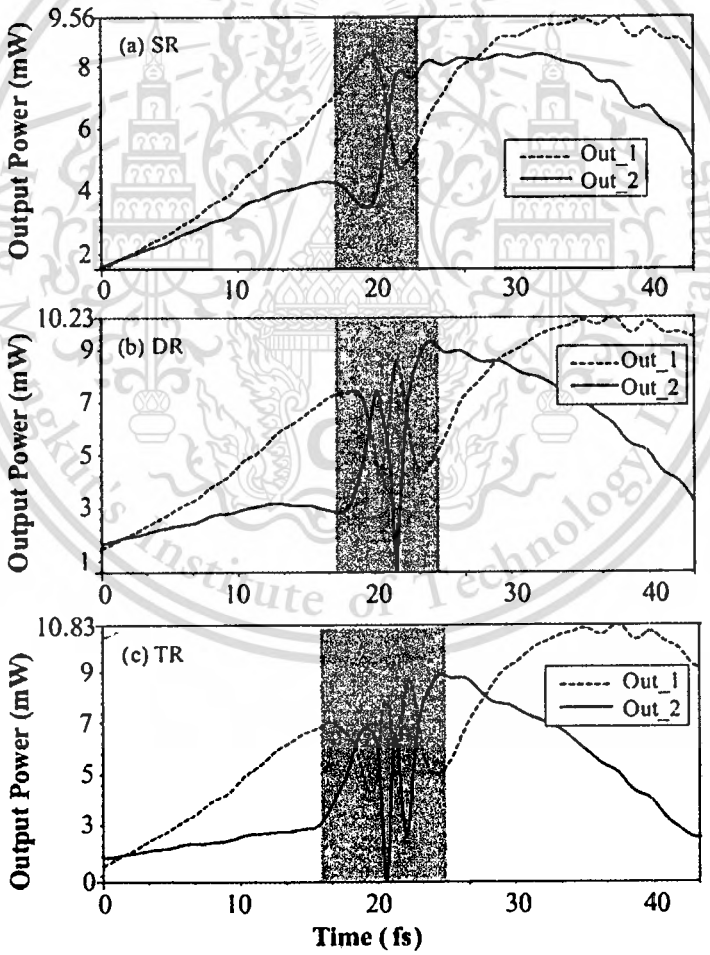

Figure 5.2 Simulation results of ultrafast switching window based on number of NMRs coupled into a MZI arm (a) single–NMR (SR), (b) double–NMR (DR) and (c) triple–NMR (TR).

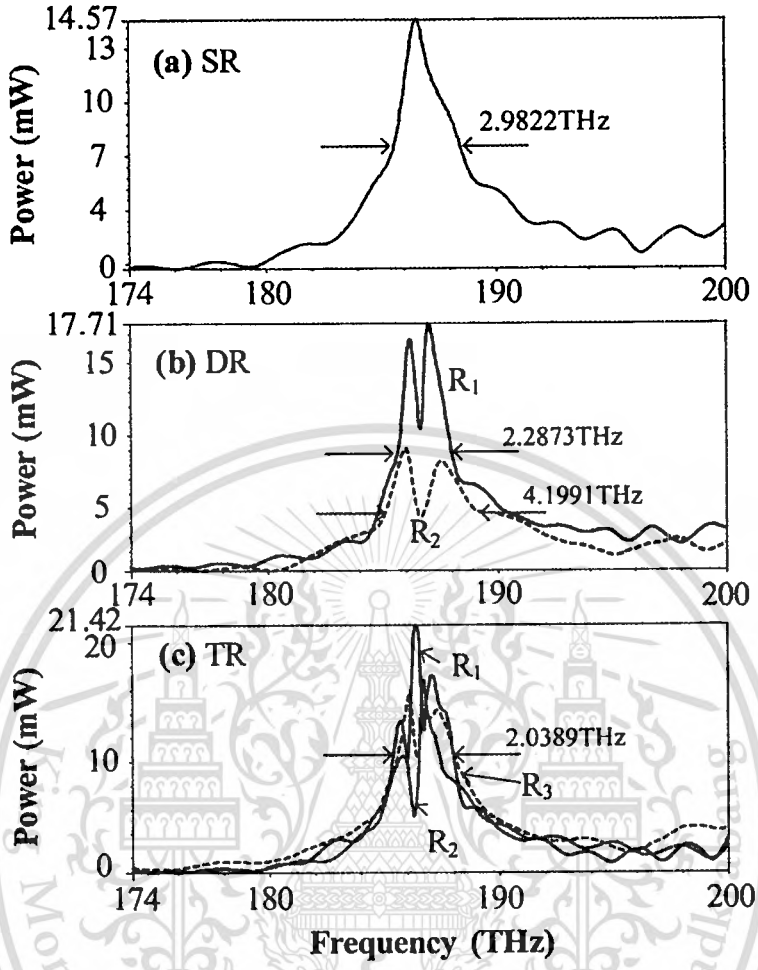

Figure 5.3 Results of low power ultrafast switching by increase the number of NMRs coupled into one MZI arm where (a) SR, (b) DR, and (c) TR.

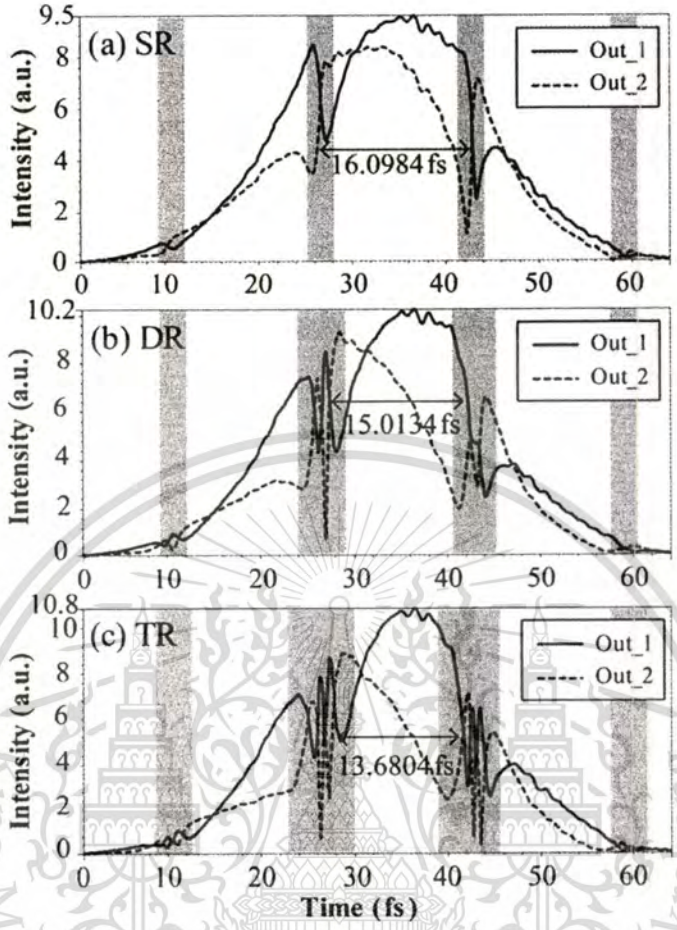

Figure 5.4 Simulation results of on–off optical switching window generation within MZI couple to number of NMR in range 161 – 224THz.

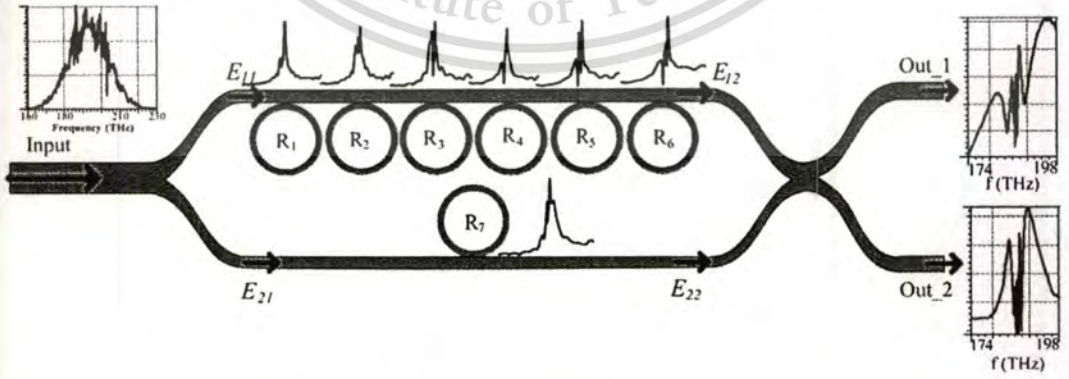

Figure 5.5 Schematic diagram of APSK generation based on seven NMRs coupled to one MZI arm, all NMRs radii R = 1.5μm.

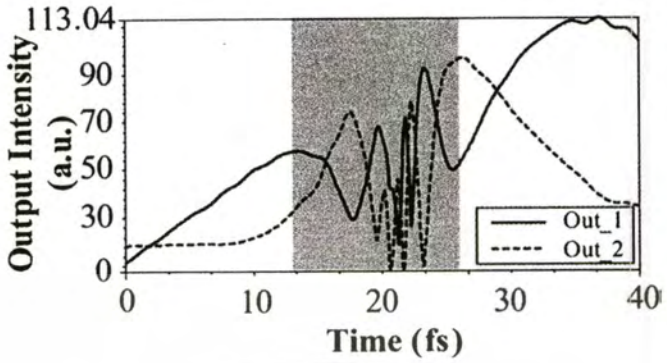

Figure 5.6 Results of ultrafast switching window based on seven NMRs coupled into a MZI arm.

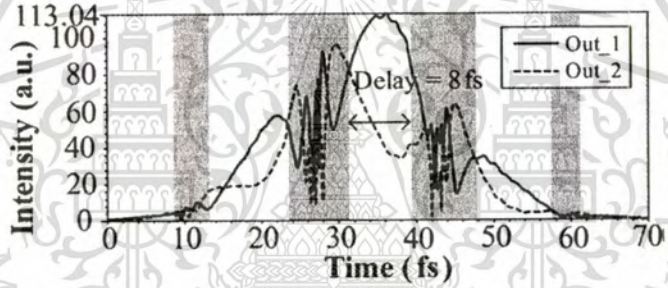

Figure 5.7 Results of packet switching based on seven NMRs coupled to a MZI arm for ultrafast packet switching use.

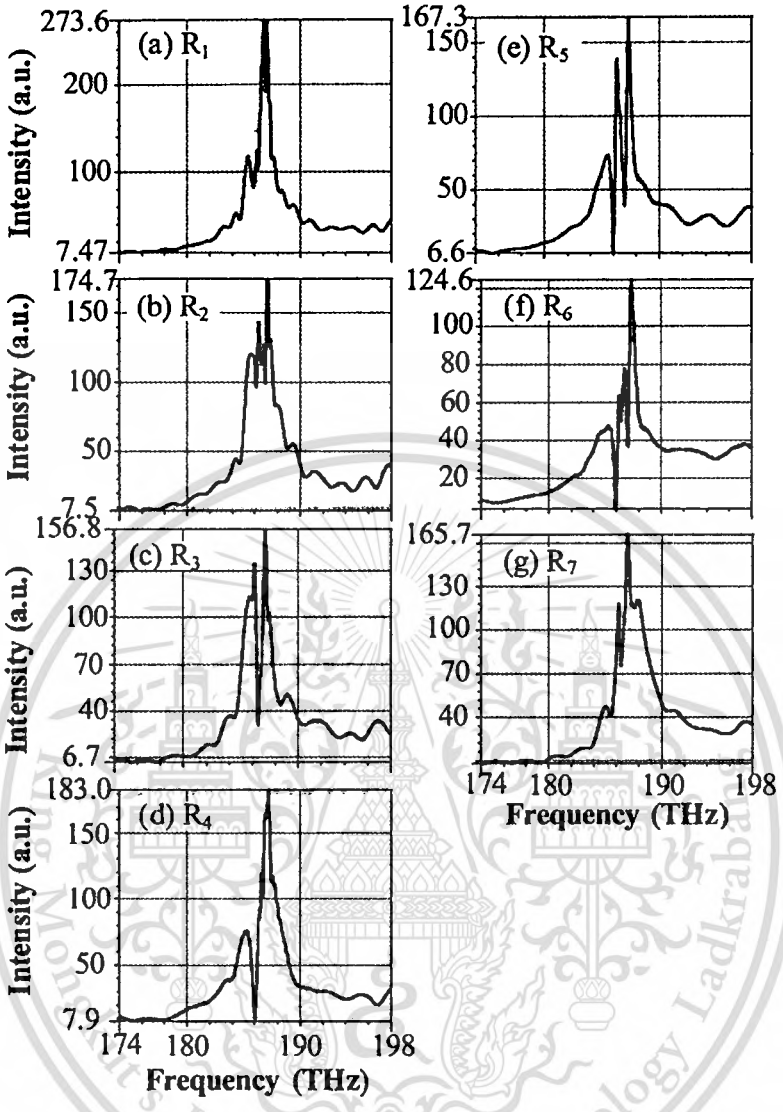

Figure 5.8 Simulation results within the microring resonators by (a) microring number 1 (R_1) (b) microring number 2 (R_2) (c) microring number 3 (R_3) (d) microring number 4 (R_4) (e) microring number 5 (R_5) (f) microring number 6 (R_6) are coupled to upper MZI arm and (g) microring number 7 (R_7) coupled to lower MZI arm.

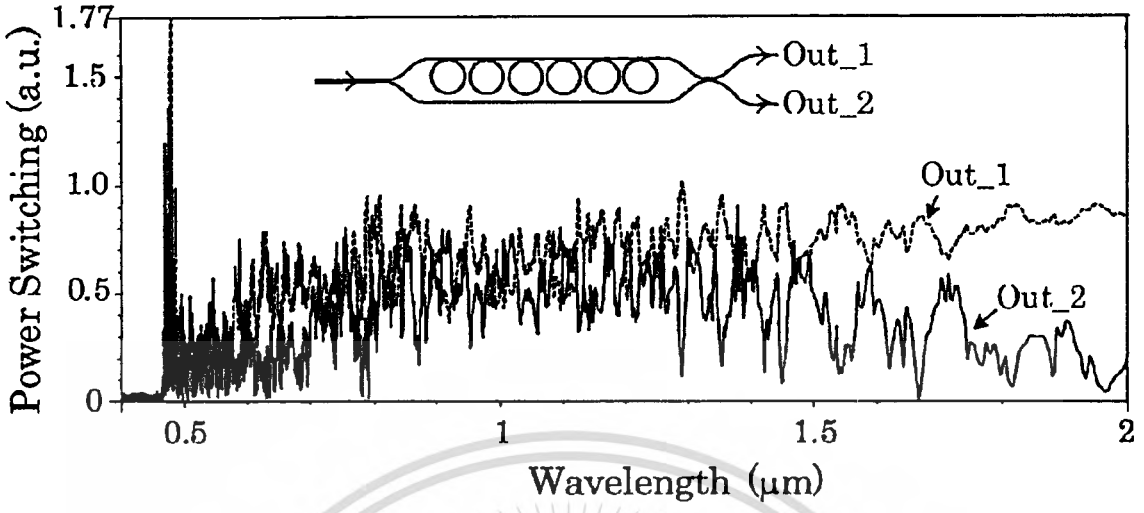

Figure 5.9 The power switching as a wavelength function of six–microring resonator (R = *1.5μm*) coupled to one MZI arm.

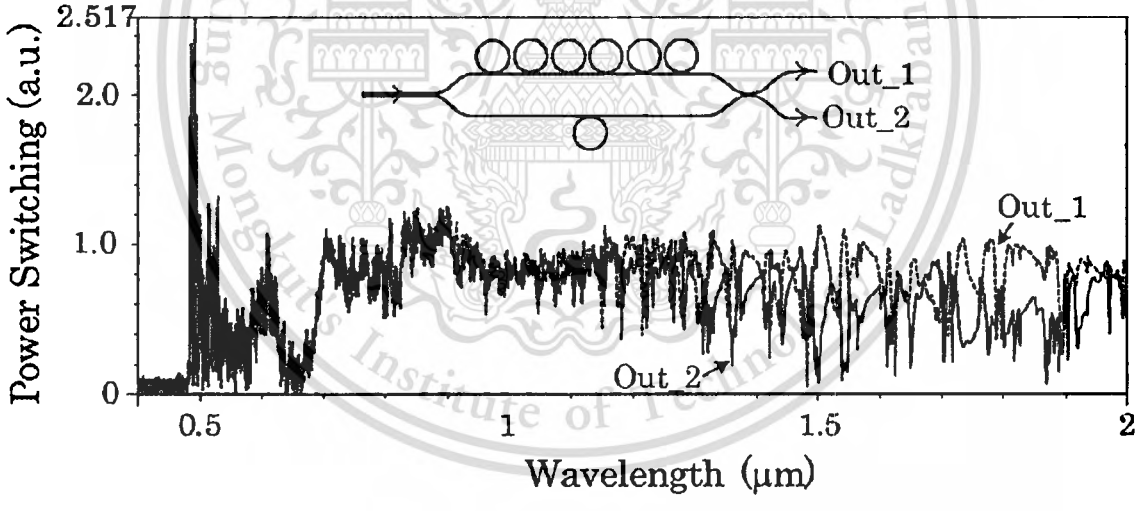

Figure 5.10 The power switching as a wavelength function of six–microring resonator (R = *1.5μm*) coupled to upper and one–microring resonator coupled to lower MZI arm.

In figure 5.9, the simulation result of power switching as a wavelength function found that the switching–on and –off between out_1 and out_2 are occurred at 0.6μm. when I added a microring

resonator coupled to lower MZI arm as shown in figure 5.10 found that the switching–on and–off between out_1 and out_2 are occurred at 1.2μm because this microring (added to lower MZI arm) is influenced phase shift keying of lower MZI arm.

5.4 Conclusions

I have proposed a new method of ultrafast switching generation based on nonlinear microring resonators coupled into a MZI arm, where both mathematical analysis and simulation results using OptiWave FDTD method [40] are obtained. By examining the switching characteristics of an optical switching block made up of nonlinear microring resonators coupled into a MZI arm, we have found that the switching speed and delay time can be increased by increasing the number of the coupling ring resonators, where in this work we found when more NMRs are coupled into the system, the faster switching time than the single–NMR is seen, where finally the packet switching delay time of 8 fs is obtained. The other advantage is that the low power all–optical ultrafast switching can be available for dense wavelength division multiplexing (DWDM) and router applications.

CHAPTER 6

CONCLUSION AND FUTURE WORK

6.1 OOK generation based on MZI incorporating a pumped nonlinear ring resonators system

The OOK modulation format by using NRRs coupled into one arm of a MZI system could be performed. The solution of the nonlinear Schrödinger equation is $E_{Li} = E_{Ri} \exp\left(-\frac{\alpha}{2} L_i - \gamma_{NL_i} |E_{Ri}|^2 L_i\right)$, which describes the nonlinear properties in each nonlinear ring resonator by using the term $|E_{Ri}|^2$ that circulates in each NRR. It is used to enhance and amplify the output signals. When the input light pulse is input through a 3dB coupler of a MZI, the coupling power is partially circulated through R_1, where it is circulated and combined with the pump light within R_1. Finally, the output of rings R_2 and R_3 are obtained in the similar manner.

The feasibility of the device by comparison to already fabricated devices with the same radius NRR radii, where $R_1 = 1.5\mu m$, $R_2 = 1.0\mu m$ *and* $R_3 = 0.775\mu m$. this parameter details are given by reference [60]. Our proposed system is the extended system of a Mach–Zehnder interferometer combined with ring resonators. It was fabricated by Rabus [61], where the system size was 700 × 2500 μm^2. It is larger than the system in this paper where the system size is 10 × 40μm^2. Moreover, our system is combined with the triple nonlinear ring resonators. Two different results at the center wavelength 1.31μm and 1.55μm are compared, where they are dominated by the nonlinear refractive indices and two–photon absorption coefficients within the NRRs. We found that the OOK generated at 1.55μm is shown the fastest switching, where the delay time of OOK is 1.2fs. We have also presented the principles of MZI operation in PSBT–based systems, where the characterization of useful parameters required for the DPSK demodulation or PSBT encoding. DPSK and PSBT have

been highlighted as the suitable modulation formats for optical transmissions. The DPSK modulation format presents the better performance for transmission than the conventional OOK, justifying its utilization. However, the DPSK requires the passive MZIs for interferometric demodulation. In application, the use of DWDM (Dense Wavelength Division Multiplexing) can be employed to obtain the multi-wavelength OOK, which may be available for high capacity packet switching.

6.2 Novel Tunable Dynamic Tweezers using Dark–Bright Solitons Collision Control in an Optical Add/Drop Filter

In this chapter, I have demonstrated that after the dark soliton pulse was generated by using the pumped laser system. I have shown that the propagating dark soliton within the MRR and NRR system can be converted to be a bright soliton by using the ring resonator system, incorporating the add/drop multiplexer, moreover, the amplification and tenability of the dark soliton pulse can be obtained. By using the reasonable dark–bright soliton input power, the tunable optical tweezers can be controlled, which can be used as the dynamic optical tweezers probe. In application, such a behavior can be used to confine the suitable size of light pulse or molecule, which can be employed in the same way of the optical tweezers. But in this case the terms dynamic probing is come to be a realistic function. Moreover, the transportation of the trapped pulse or molecule is plausible.

6.3 Low Power Ultrafast Switching Generation Based on NMRs Coupled into a MZI Arm

I have proposed a new method of ultrafast switching generation based on nonlinear microring resonators coupled into a MZI arm, where both mathematical analysis and simulation results using OptiWave FDTD method are obtained. By examining the switching characteristics of an optical

switching block made up of nonlinear microring resonators coupled into a MZI arm, we have found that the switching speed and delay time can be increased by increasing the number of the coupling ring resonators, where in this work we found when more NMRs are coupled into the system, the faster switching time than the single–NMR is seen, where finally the packet switching delay time of 8 fs is obtained. The other advantage is that the low power all–optical ultrafast switching can be available for dense wavelength division multiplexing (DWDM) and router applications.

6.4 Future Work

One of the main goals in this work was to realize random binary code generation based on microring resonators coupled to one arm MZI by using dark–bright solitons conversion control. Even though we have reached many of our targets, there is still scope for improvements and further exploration of some of the issues.

1. The spin up and down in photonics and quantum dots systems.
2. The multi electron–hole pair based on dark–bright soliton conversion.
3. The properties effect of optoelectronics based on dark–bright soliton conversion.

REFERENCES

[1] A. H. Gnauck, K.C. Reichmann, J.M. Kahn, S.K. Korotky, J.J. Veselka, and T.L. Koch, "4–Gb/s heterodyne transmission experiments using OOK, FSK, and DPSK modulation," IEEE Photon. Technol. Lett., vol. **2**, pp. 908–910, 1990.

[2] S. R. Nuccio, O. F. Yilmaz, S. Khaleghi, X. Wu, L. Christen, I. Fazal, and A. E. Willner, "Tunable 503 ns optical delay of 40 Gbit/s RZ–OOK and RZ–DPSK using a wavelength scheme for phase conjugation to reduce residual dispersion and increase delay," Opt. Letters, vol. **34**, no. 12, pp. 1903–1905, 2009.

[3] W. Astar, J. B. Driscoll, X. Liu, J. I. Dadap, W. M. J. Green, Y. A. Vlasov, G. M. Carter, and R. M. Osgood, Jr., "Conversion of 10 Gb/s NRZ–OOK to RZ-OOK utilizing XPM in a Si nanowire," Opt. Express, vol. **17**, no. 15, pp. 12987–12999, 2009.

[4] W. Hong, D. Huang, X. Zhang, and G. Zhu, "Simulation and analysis of OOK–to–BPSK format conversion based on gain–transparent SOA used as optical phase–modulator," Opt. Express, vol. **15**, no. 26, pp. 18357–18369, 2007.

[5] T. Nishitani, T. Konishi, and K. Itoh, "All–optical M–ary ASK signal demultiplexer based on a photonic analog–to–digital conversion," Opt. Express, vol. **15**, no. 25, pp. 17025–17031, 2007.

[6] K. Mishina, S. Kitagawa, and A. Maruta, "All–optical modulation format conversion from on–off–keying to multiple–level phase–shift–keying based on nonlinearity in optical fiber," Opt. Express, vol. **15**, no. 13, pp. 8444–8453, 2007.

[7] I. Kang, "Phase–shift–keying and on–off–keying with improved performances using electroabsorption modulators with interferometric effects," Opt. Express, vol. **15**, no. 4, pp. 1467–1473, 2007.

[8] Y. G. Wen, L. K. Chen, K. P. Ho, F. Tong, and W. S. Chan, "Performance verification of a variable bit–rate limiter for on–off keying (OOK) optical systems," IEEE J. Lightwave Technol., vol. **18**, no. 6, pp. 779–786, 2000.

[9] T. Mizuochi, K. Ishida, T. Kobayashi, J. Abe, K. Kinjo, K. Motoshima, and K. Kasahara, "A comparative study of DPSK and OOK WDM transmission over transoceanic distances and their performance degradations due to nonlinear phase noise," IEEE J. Lightwave Technol., vol. **21**, no. 9, pp. 1933–1942, 2003.

[10] C. Xie, L. Möller, H. Haunstein, and S. Hunsche, "Comparison of system tolerance to polarization–mode dispersion between different modulation formats," IEEE Photon. Technol. Lett., vol. **15**, no. 8, pp. 1168–1170, 2003.

[11] M. Matsumoto, "All–optical signal regeneration using fiber nonlinearity," Eur. Phys. J. Special Topics, vol. **173**, pp. 297–312, 2009.

[12] K. Croussore, C. Kim, and G. Li, "All–optical regeneration of differential phase–shift keying signals based on phase–sensitive amplification," Opt. Letters, vol. **29**, no. 20, pp. 2357–2359, 2004.

[13] A. Akhtar, L. Pavel, and S. Kumar, "Modeling interchannel FWM with walk–off in RZ–DPSK single span links," IEEE J. Lightwave Technol., vol. **26**, no. 14, pp. 2142–2154, 2008.

[14] C. Xu, X. Liu, and X. Wei, "Differential phase–shift keying for high spectral efficiency optical transmissions", IEEE J. of Select. Topics in Quantum Electron., vol. **10**, no. 2, pp. 281–293, 2004.

[15] J. Li, L. Li, J. Zhao, and C. Li, "Ultrafast, low power, and highly stable all–optical switch in MZI with two–arm–sharing nonlinear ring resonator," Opt. Communication, vol. **256**, pp. 319–325, 2005.

[16] J. E. Heebner, N. N. Lepeshkin, A. Schweinsberg, G. W. Wicks, and R. W. Boyd, "Enhanced linear and nonlinear optical phase response of AlGaAs microring resonators," Opt. Letters, vol. **29**, pp. 769–771, 2004.

[17] A. Rostami, "Low threshold and tunable all–optical switch using two–photon absorption in array of nonlinear ring resonators coupled to MZI," J. Microelectronics, vol. **37**, pp. 976–981, 2006.

[18] A. Bananej, and C. Li, "Parameter controllable all–optical switching in a high–nonlinear micro ring coupled MZI through a pumped nonlinear coupler." J. Nonlinear Opt. Phys. and Mater., vol. **14**, no. 1, pp. 85–91, 2005.

[19] S. Mitatha, "Dark soliton behaviors within the nonlinear micro and nanoring resonators and applications." Progress In Electromagnetics Research, PIER, vol. **99**, pp. 383–404, 2009.

[20] K. Svoboda and Block S. M, "Biological applications of optical forces," Annu. Rev. Biophys. Biomol. Struct., vol. **23**, pp. 247–283, 1994.

[21] A. Ashkin, J. M. Dziedzic and T. Yamane, "Optical trapping and manipulation of single cells using infrared laser beams," Nature, vol. **330**, pp. 769–771, 1987.

[22] W. Tan, J. Twomey, D. Guo, K. Madhavan, and M. Li, "Evaluation of Nanostructural, Mechanical, and Biological Properties of Collagen–Nanotube Composites," IEEE Trans. on Nanobioscience, vol. **9**, pp. 111–120, 2010.

[23] I. T. S. Li, E. Mills, and K. Truong, "A computational tool for Monte Carlo simulations of biomolecular reaction networks modeled on physical principles" IEEE Trans.on Nanobioscience, vol. **9**, pp. 24–30, 2010.

[24] J. Conia, B. S. Edwards and S. Voelkel, "The micro–robotic laboratory: optical trapping and scissing for the biologist," J. Clin. Lab. Anal., vol. **11**, pp. 28–38, 1997.

[25] G. P. Agrawal, Nonlinear Fiber Optics, Academic Press, 4th edition, New York, 2007.

[26] S. Mitatha, B. Piyatamrong, P.P. Yupapin, B. Knobnob, and S. Chaiyasoonthorn, "Optical vortices generated by light pulses within a PANDA ring resonator," J. Nonlin. Opt. Phys. Mater., vol. **20**, no. 1, pp. 85–97, 2011.

[27] H. Cai and A. Poon, "Optical manipulation and transport of microparticle on silicon nitride microring resonator–based add–drop devices," Opt. Lett., vol. **35**, no. 17, pp. 2855–2857, September, 2010.

[28] M. Brunstein, A. M. Yacomotti, R. Braive, S. Barbay, I. Sagnes, L. Bigot, L. Le–Gratiet, and J. A. Levenson, "All–optical, all–fibered ultrafast switching in 2–D InP–based photonic crystal nanocavity," J. IEEE Photon., vol. **2**, no. 4, pp. 642–651, Aug. 2010.

[29] L.–D. Haret, T. Tanabe, E.Kuramochi, and M. Notomi, "Extremely low power optical bistability in silicon demonstrated using 1D photonic crystal nanocavity," Opt. Express, vol. 17, no. 23, pp. 21108–21117, Nov. 2009.

[30] R. Takahashi, T. Yasui, J. –K. Seo, and H. Suzuki, "Ultrafast all–optical serial–to–parallel converters based on spin–polarized surface–normal optical switches," IEEE J. Select. Topics Quant. Electron., vol. **13**, no. 1, pp. 92–103, Jan. –Feb. 2007.

[31] C. Bintjas, K. Vlachos, N. Pleros, and H. Avramopoulos, "Ultrafast nonlinear interferometer (UNI)–based digital optical circuits and their use in packet switching," J. Lightw. Technol., vol. **21**, no. 11, pp. 2629–2637, Nov. 2003.

[32] N. Chi, L. Xu, J. Zhang, P. V. Holm–Nielsen, C. Peucheret, S.n Yu, and P. Jeppesen, "Improve the performance of orthogonal ASK/DPSK optical label switching by DC–balanced line encoding," J. Lightw. Techn., vol. **24**, no. 3, pp. 1082–1092, March 2006.

[33] A. Bananej and C. F. Li, "Controllable all–optical switch using an EDF–ring coupled M–Z interferometer," IEEE Photon. Technol. Lett., vol. **16**, pp. 2102–2104, Sept. 2004.

[34] L. Y. Mario, S. Darmawan, and M. K. Chin, "Asymmetric Fano resonance and bistability for high extinction ratio, large modulation depth, and low power switching," Opt. Express, vol. **14**, pp. 12770–12781, 2006.

[35] M. C. Hoffmann, B.S. Monozon, D. Livshists, E.U. Rafailov, and D. Turchinovich, "Terahertz electro–absorption effect enabling femtosecond all–optical switching in semiconductor quantum dots," Appl. Phys. Lett., vol. **97**, 231108, 2010.

[36] M. Bulters, M. Breede, M. Hofmann, and D. Jager, "Nonasecond switching and wavelength tuning of external–cavity laser diode using a reflective electroabsorption modulator," IEEE Photon. Technol. Lett., vol. **21**, no. 18, pp. 1347–1349, Sep. 2009.

[37] C. –Y. Jin, O. Kojima, T. Inoue, T. Kita, O. Wada, M. Hopkinson, and K. Akahane, "Detailed design and characterization of all–optical switches based on InAs/GaAs quantum dots in a vertical cavity," IEEE J. Quant. Electron., vol. **46**, no. 11, pp. 1582–1589, Nov. 2010.

[38] Y.Z. Hu, D.S. Ang, and Z.Q. Teo, "Threshold voltage and mobility extraction by ultrafast switching measurement on NBTI," IEEE Trans. Electron Dev., vol. **57**, no. 8, pp. 2027–2031, Aug. 2010.

[39] P. P. Yupapin, and C. Teeka, "OOK generation based on MZI incorporating a pumped nonlinear ring resonators system," Opt. Express, vol. **18**, no. 8, pp. 9891–9899, Apr. 2010.

[40] OptiFDTD by OptiWave Corp. ©, ver. 8.0, single license (KMITL), 2008.

[41] K. Sarapat, N. Sangwara, K. Srinuanjan, P.P. Yupapin and N. Pornsuwancharoen, "Novel dark–bright optical solitons conversion system and power amplification," Opt. Eng., vol. **48**, pp. 045004, 2009.

[42] S. Mitatha, N. Pornsuwancharoen and P.P. Yupapin, "A simultaneous short–wave and millimeter–wave generation using a soliton pulse within a nano–waveguide," IEEE Photon. Technol. Lett., vol. **21**, pp. 932–934, 2009.

[43] A. Charoenmee, N. Pornsuwancharoen and P.P.Yupapin, "Trapping a dark soliton pulse within a nano ring resonator," Int. J. Light Electron Opt., vol. **121**, no. 18, pp. 1670–1673, 2010.

[44] M.E. Heidari, M.K. Moravvej–Farshi, and A. Zariffkar, "Multichannel wavelength conversion using fourth–order soliton decay," J. Lightwave Technol., vol. **25**, pp. 2571–2578, 2007.

[45] L. Yuan, Z. Liu, J. Yang and C. Guan, "Twin–core fiber optical tweezers," Optics Express, vol. **16**, pp. 4559–4566, 2008.

[46] N. Malagninoa, G. Pescea, A. Sassoa and E. Arimondo, "Measurements of trapping efficiency and stiffness in optical tweezers," Opt. Commun., vol. **214**, pp. 15–24, 2002.

[47] G. Brambilla, G. Senthil Murugan, J.S. Wilkinson, and D.J. Richardson, "Optical manipulation of microspheres along a subwavelength optical wire," Opt. Lett., vol. **32**, pp. 3041–3043, 2007.

[48] C. Fietz and G. Shvets, "Nonlinear polarization conversion using microring resonators," Opt. Lett., vol. **32**, pp. 1683–1685, 2007.

[49] Y. Kokubun, Y. Hatakeyama, M. Ogata, S. Suzuki and N. Zaizen, "Fabrication technologies for vertically coupled microring resonator with multilevel crossing busline and ultracompact–ring radius," IEEE J. Sel. Top. Quantum Electron., vol. **11**, pp 4–10, 2005.

[50] A. Ashkin, J.M. Dziedzic, J.E. Bjorkholm and S. Chu, "Observation of a single–beam gradient force optical trap for dielectric particles," Opt. Lett., vol. **11**, pp. 288–290, 1986.

[51] S. Bergamini, B. Darqui, M. Jones, L. Jacubowiez, A. Browaeys and P. Grangier, "Holographic generation of microtrap arrays for single atoms by use of a programmable phase modulator", J. Opt. Soc. Am. B, vol. **21**, pp. 1889–1894, 2004.

[52] D. D. Yavuz, P. B. Kulatunga, E. Urban, T. A. Johnson, N. Proite, T. Henage, T. G. Walker and M. Saffman, "Fast ground state manipulation of neutral atoms in microscopic optical traps", Phys. Rev. Lett., vol. **96**, 063001, 2006.

[53] D. Schrader, I. Dotsenko, M. Khudaverdyan, Y. Miroshnychenko, A. Rauschenbeutel and D. Meschede, "Neutral atom quantum register", Phys. Rev. Lett., vol. **93**, 150501, 2004.

[54] J. A. Sauer, K. M. Fortier, M. S. Chang, C. D. Hamley and M. S. Chapman, Submicrometer position control of single trapped neutral atoms, Phys. Rev. A, vol. **69**, 051804(R), 2004.

[55] T. P. Meyrath, F. Schreck, J. L. Hanssen, C.-S. Chuu and M. G. Raizen, "Bose–Einstein condensate in a box," Phys. Rev. A, vol. **71**, 041604(R), 2005.

[56] V. Boyer, R. M. Godun, G. Smirne, D. Cassettari, C. M.Chandrashekar, A. B. Deb, Z. J. Laczik and C. J. Foot, "Dynamic manipulation of Bose–Einstein condensates with a spatial light modulator", Phys. Rev. A, vol. **73**, 031402(R), 2006.

[57] A.V. Carpentier, J. Belmonte-Beitia, H. Michinel and V.M. Perez–Garcia, "Laser tweezers for atomic solitons," J. of Mod. Opt., vol. **55**, no. 17, pp. 2819–2829, 2008.

[58] V. Milner, J. L. Hanssen, W. C. Campbell and M. G.Raizen, "Optical billiards for atoms," Phys. Rev. Lett., vol. **86**, pp. 1514–1516, 2001.

[59] N. Friedman, A. Kaplan, D. Carasso and N. Davidson, "Observation of chaotic and regular dynamics in atom-optics billiards," Phys. Rev. Lett., vol. **86**, pp. 1518–1520, 2001.

[60] M. Li and J. Arlt, "Trapping multiple particles in single optical tweezers", Opt. Commun., vol. **281**, pp. 135–140, 2008.

[61] M. Schulz, H. Crepaz, F. Schmidt-Kaler, J. Eschner and R. Blatt, "Transfer of trapped atoms between two optical tweezer potentials" J. of Mod. Opt., vol. **54**, no. 11, pp. 1619–1626, 2007.

[62] D.G. Rabus, M. Hamacher, and H. Heidrich, "Resonance frequency tuning of a double ring resonator in GaInAsP/InP: Experiment and simulation," Jpn. J. Appl. Phys., vol. **41**, pp. 1186–1189, 2002.

[63] D. G. Rabus, *Integrated Ring Resonators*, (Springer–Verlag Berlin Heidelberg). Chap. 5.4, pp. 169–173, 2007.

[64] OptiFDTD finite difference time domain photonics simulation software, OptiWave systems Inc. © 2008, http://www.optiwave.com/

APPENDIX

List of Publications

Publications in 2009

1. **Chat Teeka**, Panuwat Chaiyachet, and Preecha P. Yupapin, "Soliton collision management in a microring resonator system," *Physics Procedia*, vol. **2**, no. 1, pp. 67–73, July 2009.

Publications in 2010

1. P. P. Yupapin, and **Chat Teeka**, "OOK generation based on MZI incorporating a pumped nonlinear ring resonators system," *Optics Express*, vol. 18, no. 8, pp. 9891–9899, 12 April 2010. (IF 2009: 3.88)
2. **C. Teeka**, Muhammad Arif Jalil, Preecha P. Yupapin and Jalil Ali, "Novel tunable dynamic tweezers using dark–bright solitons collision control in an optical add/drop filter," *IEEE Transection on Nanobioscience*, vol. **9**, no. 4, pp. 1–9, Dec. 2010. (IF 2009: 1.705)
3. P. Youplao, T. Phattaraworamet, S. Mitatha, **C. Teeka**, and P. P. Yupapin, "Novel optical trapping tool generation and storage controlled by light," *Journal of Nonlinear Optical Physics and Materials,* vol. 19, no. 2, pp. 371–378, June 2010. (IF 2008: 0.667)
4. T. Phatharaworamet, **C. Teeka**, R. Jomtarak, S. Mitatha, and P. P. Yupapin, "Random binary code generation using dark–bright soliton conversion control within a PANDA ring resonator," *J. Lightwave Technology*, vol. 28, no. 19, pp. 2804–2809, October 2010. (IF 2009: 2.165)
5. N. Sangwara, **C. Teeka**, S. Pipatsart, P.P. Yupapin, "An investigation of dark soliton behaviors within the nonlinear micro and nano ring resonators," *Optik –International Journal for Light and Electron Optics*, vol. 121, no. 21, pp. 1959 – 1961, November 2010. (IF 2009: 0.378)

6. Metha Tasakorn, **Chat Teeka**, Rangsan Jomtarak, and Preecha P. Yupapin, "Multitweezers generation control within a nanoring resonator system," *Optical Engineering*, vol. **49**, no. 7, 075002, July 2010. (IF 2009: 0.553)
7. B. Jukgoljun, N. Suwanpayak, **C. Teeka** and P.P. Yupapin, "Hybrid transceiver and repeater using a PANDA ring resonator for nano communication" *Optical Engineering*, vol. **49**, no. 12, 125003, 2010. (IF 2009: 0.553)
8. M. A. Jalil, I. S. Amiri, **C. Teeka**, J. Ali and P. P. Yupapin, "All–optical Logic XOR/XNOR Gate Operation using Microring and Nanoring Resonators," *Physics Express*, vol. 1(1), pp. 15–22, 2010. (invited paper)
9. P. P. Yupapin, N. Suwanpayak, B. Jukgoljun and **C. Teeka**, "Hybrid Transceiver using a PANDA Ring Resonator for Nano Communication," *Physics Express*, vol. 1, no. 1, pp. 1–8, 2010. (invited paper)

Publications in 2011

1. N. Suwanpayak, M. A. Jalil, **Chat Teeka**, J. Ali, and P. P. Yupapin, "Optical vortices generated by a PANDA ring resonator for drug trapping and delivery applications," *Biomedical Optics Express*, vol. **2**, no. 1, pp. 159–168, January 2011.
2. P. Phongsanam, **C. Teeka**, S. Mitatha, and P. P. Yupapin, "Simultaneous all–optical logic AND and OR gates based on photonic circuits," *Optics and Photonics Letters*, vol. 4, No. 1, pp. 17–24, 2011.
3. P. Pongwongtragull, **C. Teeka**, S. Kamoldilok and P.P. Yupapin, "Novel communication security scheme using dark–bright soliton conversion behaviors," *Optical Eng*ineering, vol. **50**, no. 2, 025004, 2011. (IF 2009: 0.553)

4. P. Phongsanam, S. Mitatha, **C. Teeka** and P.P. Yupapin, "All optical half adder/subtractor using dark–bright soliton conversion control," *Microwave and Optical Technology Letters*, vol. 53, no. 7, pp. 1541–1544, 2011. (IF 2009:0.685)

5. M.A. Jalil, N. Suwanpayak, **C. Teeka**, P.P. Yupapin, J. Ali, "Molecular buffer, storage and delivery using a PANDA ring resonator and an optical router," *Recent Patent on Computer Science*, vol. 4, no. 1, pp. 77–79, 2011.

6. S. Punthawanunt, **C. Teeka**, R. Jomtarak, and P. P. Yupapin, "Simulation of an optical buffer using microring resonator array with 1.5μm radius," *Procedia Engineering*, vol. 8, pp. 428–431, 2011.

7. C. Tanaram, **C. Teeka**, R. Jomtarak, P. P. Yupapin , M. A. Jalil, I. S. Amiri, and J. Ali, "ASK–to–PSK generation based on nonlinear microring resonators coupled to one MZI arm," *Procedia Engineering*, vol. 8, pp. 432–435, 2011.

8. S. Punthawanunt, **C. Teeka**, R. Jomtarak, and P. P.Yupapin, "An optical buffer manipulation using a microring array," *Procedia Engineering*, vol. 8, pp. 441–444, 2011.

9. S. Punthawanunt, **C. Teeka**, R. Jomtarak, S. Mitatha, J. Ali, and P. P. Yupapin, "A new concept of multi electron–hole pair generation using dark–bright soliton conversion control," *Procedia Engineering*, vol. 8, pp. 483–486, 2011.

10. S. Punthawanunt, R. Jomtarak, **C. Teeka**, P. P. Yupapin, and J. Ali, "Single electron–hole pair generation using dark–bright solitons conversion control," *Procedia Engineering*, vol. 8, pp. 493–497, 2011.

11. M. A. Jalil, **C. Teeka**, J. Ali and P. P. Yupapin, "Mathematical modeling of light pulse within linear and nonlinear ring resonators, " *Pioneer Journal of Advances in Applied Mathematics*, vol. 1, no. 1, pp. 1–57, 2011.

12. N. Suwanpayak, **C. Teeka**, and P.P. Yupapin, Hybrid transistor manipulation controlled by light, *Microwave and Optical Technology Letters*, vol. 53, no. 11, 2533–2537, Nov. 2011. (IF 2010: 0.656)

13. F. D. Ismail, R. Jomtarak, **C. Teeka**, J. Ali, and P.P. Yupapin, All–optical switches based on GaAs/AlGaAs quantum dots vertical cavity, *Journal of Nonlinear Optical Physics and Materials*, vol. 20, no. 2, pp. 205–215, 2011. (IF 2010: 0.553)

14. **C. Teeka**, S. Songmuang, R. Jomtarak, P. P. Yupapin, M. A. Jalil, I. S. Amiri, and J. Ali, "ASK–to–PSK generation based on nonlinear microring resonators coupled to one MZI arm," *AIP Conferences Proceeding*, **1341**, 221 (2011)

15. R. Jomtarak, **C. Teeka**, P. P. Yupapin, and J. Ali, "Single electron–hole pair generation using dark–bright solitons conversion control," *AIP Conferences Proceeding*, **1341**, 228 (2011).

16. S. Punthawanunt, **C. Teeka**, R. Jomtarak, S. Mitatha, J. Ali and P. P. Yupapin, "A new concept of multi electron–hole pair generation using dark–bright soliton conversion control," *AIP Conferences Proceeding*, **1341**, 231 (2011).

Proceedings/Conferences List

1. P. Limpaibool, S. Mitatha, **C. Teeka**, R. Jomtarak and P.P. Yupapin, "Novel optical tweezers storage within add/drop optical filter using dark–bright solitons conversion control," Conferences on defense, Kuala Lumpur, Malaysia, 2009.

2. **C. Teeka**, S. Songmuang, R. Jomtarak, P. P. Yupapin, M. A. Jalil, I. S. Amiri, and J. Ali, "ASK–to–PSK generation based on nonlinear microring resonators coupled to one MZI arm," *AIP Conferences Proceeding*, **1341**, 221 (2011). [Nanotech Malaysia 2010: International Conference on Enabling Science and Nanotechnology (ESciNano), Kuala Lumpur, Malaysia. 1–3 Dec. 2010.]

3. R. Jomtarak, **C. Teeka**, P. P. Yupapin, and J. Ali, "Single electron–hole pair generation using dark–bright solitons conversion control," *AIP Conferences Proceeding*, **1341**, 228 (2011). [Nanotech Malaysia 2010: International Conference on Enabling Science and Nanotechnology (ESciNano), Kuala Lumpur, Malaysia. 1–3 Dec. 2010.]

4. S. Punthawanunt, **C. Teeka**, R. Jomtarak, S. Mitatha, J. Ali and P. P. Yupapin, "A new concept of multi electron–hole pair generation using dark–bright soliton conversion control," *AIP Conferences Proceeding*, **1341**, 231 (2011). [Nanotech Malaysia 2010: International Conference on Enabling Science and Nanotechnology (ESciNano), Kuala Lumpur, Malaysia. 1–3 Dec. 2010.]

5. Sa-nga Songmuang, **Chat Teeka**, Rangsan Jomtarak, and Preecha P. Yupapin, "High capacity packet switching using nanoring resonator incorporating a MZI," 3rd Joint International Conference on Information & Communication Technology Electronic and Electrical Engineering (JICTEE–2010) in the period Tuesday 21 – Friday 24 December 2010, in Luangprabang, Lao PDR.

6. Khunlux Mitsophonsiri, **Chat Teeka**, Rangsan Jomtarak, and Preecha P. Yupapin, "An investigation of strong and weak perturbation within a PANDA ring system," 3rd Joint International Conference on Information & Communication Technology Electronic and Electrical Engineering (JICTEE–2010) in the period Tuesday 21 – Friday 24 December 2010, in Luangprabang, Lao PDR.

7. Somchai Tangsathityangkul, Suphanchi Punthawanunt, **Chat Teeka**, Rangsan Jomtarak, and Preecha P. Yupapin, "Resonant peak pependence of a microring resonator gap coupling effects," 3rd Joint International Conference on Information & Communication Technology Electronic and Electrical Engineering (JICTEE–2010) in the period Tuesday 21 – Friday 24 December 2010, in Luangprabang, Lao PDR.

8. Suphanchai Punthawanunt, **Chat Teeka**, Rangsan Jomtarak, and Preecha P. Yupapin, "An optical buffer manipulation using a microring array," 3rd Joint International Conference on Information & Communication Technology Electronic and Electrical Engineering (JICTEE–2010) in the period Tuesday 21 – Friday 24 December 2010, in Luangprabang, Lao PDR.
9. Boonying Knobnob, Preecha P. Yupapin, R. Jomtarak, **Chat Teeka**, Somsak Mitatha, and Sawatsakorn Chaiyasoonthorn, "ASK–to–PSK generation based on nonlinear microring resonators coupled to one MZI arm," The Forth International Conference on Modelling and Simulation (ICMS–2011) in the period 24 – 27 April 2011, in Pukhet, Thailand.
10. Somsak Mitatha, Preecha P. Yupapin, R. Jomtarak, **Chat Teeka**, Sawatsakorn Chaiyasoonthorn, Sappasit Thongmee, and Boonying Knobnob, "Mathematical simulation of dielectric mirror modeling," The Forth International Conference on Modelling and Simulation (ICMS–2011) in the period 24 – 27 April 2011, in Pukhet, Thailand.

Books

1. P.P. Yupapin, **C. Teeka**, M. A. Jalil, and J. Ali, ***Nanoscale PANDA Ring Resonator***, CRC Press: Science Publishers, Taylor & Francis Group Co., 2011.
2. P.P. Yupapin, S. Mitatha, J. Ali, and **C. Teeka**, ***Nanocommunication Networks***, NOVA Science Publishers, Inc., New York, 2011.

BIOGRAPHY

Author	Chat Teeka
Date of Birth	August 6, 1976
Place of Birth	Ubonratchathani, Thailand
E-mail	chat_tee@dusit.ac.th
Bachelor Degree	B. Sc. (Physics) from Ubonratchathani University, Thailand
Year of Graduation	2000
Master Degree	M. Sc. (Applied Physics)
Institution	King Mongkut's Institute of Technology Landkrabang, Bangkok, Thailand, in 2006
Contact Address	Scientific Equipment Center, Faculty of Science and Technology, Suan Dusit Rajabhat University, Bangkok 10700, Thailand

CHAT TEEKA is currently a research staff in the department, and heading for his higher education in the interested areas. His research interests are nonlinear optics, nonlinear communication, nano–waveguide, optical soliton (dark–bright soliton conversion both theory and applications), modulation format, OOK, ASK, FSK, PSK, nonlinear phenomena in microring resonator, PANDA ring and microring coupled to MZI (such as bistability, instability, chaos, FWM), all-optical logic gates, electron-hole pair manipulation, hybrid photonic transistors (single–photon transistor, single–atom transistor, single–electron transistor, single–molecule transistor), random binary code, all–optical signal processing, all–optical switching, optical tweezer, all–optical trapping and manipulation, RF photonic, nanoscale in photonic, photonic sensors, optoelectronics, and quantum information and computing.